ADVANCED REVIEW

Nanoparticle contrast agents for X-ray imaging applications

Jessica C. Hsu[1,2] | Lenitza M. Nieves[1,3] | Oshra Betzer[4] | Tamar Sadan[4] | Peter B. Noël[1] | Rachela Popovtzer[4] | David P. Cormode[1,2,3]

[1]Department of Radiology, Perelman School of Medicine of the University of Pennsylvania, Philadelphia, Pennsylvania

[2]Department of Bioengineering, School of Engineering and Applied Science of the University of Pennsylvania, Pennsylvania

[3]Department of Biochemistry and Molecular Biophysics, Perelman School of Medicine of the University of Pennsylvania, Philadelphia, Pennsylvania

[4]Faculty of Engineering and the Institute of Nanotechnology and Advanced Materials, Bar-Ilan University, Ramat Gan, Israel

Correspondence
David P. Cormode, Departments of Radiology, Bioengineering, and Biochemistry and Molecular Biophysics, Perelman School of Medicine of the University of Pennsylvania, 3400 Spruce Street, 1 Silverstein, Philadelphia, PA 19104.
Email: david.cormode@pennmedicine.upenn.edu

Abstract

X-ray imaging is the most widely used diagnostic imaging method in modern medicine and several advanced forms of this technology have recently emerged. Iodinated molecules and barium sulfate suspensions are clinically approved X-ray contrast agents and are widely used. However, these existing contrast agents provide limited information, are suboptimal for new X-ray imaging techniques and are developing safety concerns. Thus, over the past 15 years, there has been a rapid growth in the development of nanoparticles as X-ray contrast agents. Nanoparticles have several desirable features such as high contrast payloads, the potential for long circulation times, and tunable physicochemical properties. Nanoparticles have also been used in a range of biomedical applications such as disease treatment, targeted imaging, and cell tracking. In this review, we discuss the principles behind X-ray contrast generation and introduce new types of X-ray imaging modalities, as well as potential elements and chemical compositions that are suitable for novel contrast agent development. We focus on the progress in nanoparticle X-ray contrast agents developed to be renally clearable, long circulating, theranostic, targeted, or for cell tracking. We feature agents that are used in conjunction with the newly developed multi-energy computed tomography and mammographic imaging technologies. Finally, we offer perspectives on current limitations and emerging research topics as well as expectations for the future development of the field.

This article is categorized under:
Diagnostic Tools > in vivo Nanodiagnostics and Imaging
Nanotechnology Approaches to Biology > Nanoscale Systems in Biology

KEYWORDS

cell tracking, CT, dual-energy mammography, long circulating, nanoparticles, renal clearance, targeted agents, theranostics, X-ray imaging

1 | INTRODUCTION

Medical imaging aims to improve patient outcomes by providing key information that leads to early detection, diagnosis, and appropriate treatment of diseases. Among all the available diagnostic imaging methods, X-ray based imaging techniques remain the dominant medical imaging technology owing to their wide clinical availability, high spatial

resolution, fast image acquisition, and low cost. These imaging techniques rely on the use of X-rays, a form of ionizing electromagnetic radiation, to generate contrast based on differential tissue dependent X-ray attenuation properties. Since its first development in the early 1970s, computed tomography (CT) has become a widely used clinical X-ray imaging modality (Hounsfield, 1973). Other common types of X-ray imaging techniques being used in medicine today include radiography, mammography, and fluoroscopy. In addition, X-ray micro-CT as well as phase-contrast and dark-field CT have recently received growing interest as preclinical research tools mainly for imaging small animals (Gundogdu, Nirgianaki, Che Ismail, Jenneson, & Bradley, 2007).

Several tissue types, such as bones and lungs, are easily detected by X-ray imaging without the use of contrast agents. However, X-ray attenuating contrast media, such as those based on iodine and barium sulfate, is often needed for imaging soft tissues since X-ray imaging techniques struggle to distinguish soft tissues. For example, iodinated agents are administered intravascularly in fluoroscopic angiography to better visualize blood flow and delineate vascular systems and other organs, while barium suspensions are introduced orally to enable gastrointestinal (GI) tract imaging with CT (Oliva et al., 2012). Both of these contrast agents have been used in clinical medicine since the 1950s, but they suffer from several drawbacks, particularly iodinated small molecules, which restrict their use to only a few imaging applications. Some drawbacks include nonspecific biodistribution, short blood half-lives, and contra-indication for use with renal insufficiency (Dean, Kivisaari, & Kormano, 1983; Tepel, Aspelin, & Lameire, 2006). Most importantly, these agents are not optimized for many newly emerging X-ray imaging technologies such as dual-energy mammography (DEM) and spectral photon-counting CT (SPCCT) (Karunamuni, Tsourkas, & Maidment, 2014; Si-Mohamed et al., 2017). Given these limitations, significant effort has been devoted to developing alternative X-ray contrast agents, most of which are nanoparticle-based formulations with novel chemical compositions.

The earliest reports of nanoparticle X-ray agents were based on emulsions or liposomes containing iodinated lipids or oils, or clinically approved iodinated molecules (Elrod, Partha, Danila, Casscells, & Conyers, 2009; Hallouard, Anton, Choquet, Constantinesco, & Vandamme, 2010; Mukundan et al., 2006; Torchilin, Frank-Kamenetsky, & Wolf, 1999). There now is a much more extensive array of nanoparticle imaging agents based on X-ray contrasting elements such as gold, silver, tantalum, bismuth, lanthanides, and so forth (Brown et al., 2014; Karunamuni et al., 2016; J. Kim et al., 2018; Si-Mohamed et al., 2018). Moreover, synthetic control over the composition, size, shape, and surface chemistry of these agents can greatly influence their pharmacokinetics, biodistribution, and suitability for various biomedical applications (Bouché et al., 2020; Cormode, Naha, & Fayad, 2014; J. Kim et al., 2019). For example, gold nanoparticle (AuNP) CT contrast agents of different sizes were found to have widely varying target binding affinities, circulation times, and biodistribution profiles, although their size was found to have no effect on inherent CT contrast generation (Y. C. Dong, Hajfathalian, et al., 2019; Jackson, Periasamy, Bansal, & Geso, 2011; Ross, Cole, Tilley, & Roeder, 2014). Nanoparticles can be synthesized with different coatings that yield the desired circulation times, solubility, and biocompatibility. Furthermore, the core and coating layers can be modified to include other functionalities, such as therapeutic effects with drugs or molecular imaging via targeting moieties (Ashton et al., 2018; Cormode et al., 2008; Hainfeld et al., 2011). Other contrast generating moieties can also be incorporated to provide contrast for multiple imaging modalities, such as DEM, CT, MRI, and fluorescence (Jarzyna et al., 2010; M. Liu, Anderson, Lan, Conti, & Chen, 2020). Lastly, nanoparticles can be designed to gradually degrade and release their payload for excretion (Cheheltani et al., 2016), thus minimizing the concentration of nanoparticles (i.e., dose-dependent toxicity) at the filtration site at any given time (F. Wang et al., 2009), which may be beneficial for patients with impaired renal function.

As new types of X-ray imaging techniques and relevant contrast agents are emerging, this review provides an in-depth account of developments in this field over the last 15 years. In the following sections, we will outline the basic principles of X-ray contrast production and advances in X-ray imaging technologies. We will briefly introduce small molecule-based X-ray agents and then focus on the development of novel nanoparticle X-ray contrast agents. We will include examples of renally cleared agents, long circulating agents, theranostic agents, targeted agents, cell tracking, and agents used in conjunction with new X-ray imaging modalities. Lastly, we will discuss the challenges and future perspectives on the field.

2 | X-RAY IMAGING TECHNOLOGY

2.1 | History of X-ray imaging technology

The discovery of X-rays by Wilhelm C. Röntgen in 1895 led to an important breakthrough in the field of medical imaging and diagnostics. Soon after its invention, X-ray radiography became an essential part of clinical care, especially for

diagnosing chest and bone fractures. By 1901, Dr Röntgen was awarded the first Nobel Prize in Physics for his efforts. From the early 1920s to the late 1950s, X-ray fluoroscopy and angiography were introduced to image moving body structures and visualize the vasculature, respectively. It was during this time that radiopaque agents, that were formed from elements such as iodine and barium, became increasingly utilized in X-ray imaging techniques. A major innovation in X-ray imaging was the development of X-ray CT, or 3D image slices, in 1972 by Godfrey N. Hounsfield and Allan M. Cormack (Hounsfield, 1973). Since then, there have been notable advances in CT technology, with progression of conventional single-source CT to multi-detector, multi-energy CT scanners such as SPCCT (Cormode et al., 2017). Similar technological advancement has been seen in the field of X-ray mammography during the last two decades with the recent development of DEM and spectral photon-counting mammography (Lau et al., 2018; Weigel et al., 2014).

2.2 | Principles of X-ray contrast generation

The requirements of different clinical X-ray applications, such as conventional radiography, mammography, or CT, have a significant influence on the design of their X-ray tubes. However, for all X-ray tubes, the essential components remain the same. X-rays can be generated by directing electrons at a heavy material (anode). In an X-ray tube, electrons are accelerated from the cathode to the anode in an electric field. Only 1–2% of the electrons come close enough to the nucleus to cause an interaction (Behling, 2015). These electrons, whose acceleration is sufficiently high, are decelerated in the electric field of the atomic nuclei of the anode material (e.g., molybdenum or tungsten). As a result of the deceleration process, part of the kinetic energy of the electron is converted into X-ray photons called Bremsstrahlung. On the contrary, for characteristic radiation, electrons are knocked out of their shell when an accelerated electron comes into contact. During the collision, the applied energy is transmitted by the incoming electron. The result is an ionization of the atom and a short-term vacant space in the K shell. An electron will immediately fill this vacant space from a higher energy shell, and the energy is released as characteristic X-ray photons. The emitted X-ray spectrum is therefore usually composed of a continuous spectrum (Bremsstrahlung) and a line spectrum (characteristic radiation). After leaving the tube, the X-ray spectrum is filtered to reduce low-energy radiation components, which would only increase patient dose without providing diagnostic information.

The filtered X-ray beam is directed at the subject and some of its intensity is lost (i.e., X-ray attenuation) due to two separate interactions with matter (Figure 1a,b): the photoelectric effect and Compton scattering (Lee, Choi, & Hyeon, 2013). In the case of the photoelectric effect, a photon collides with and releases all of its energy to an electron. The electron leaves the atomic network and thereby loses its atomic bond. The atom becomes ionized, and the photon is absorbed. This interaction is also known as absorption. The photoelectric effect typically scales with Z^3 (Z = atomic number) for a given photon energy and once that energy is above the K-edge of the element, or a sudden increase in X-ray absorption occurring at a photon energy level just above the binding energy of the innermost electron shell of an atom. Compton scattering, in contrast, occurs when a photon collides with and gives only part of its energy to an electron. The energy is high enough so that the electron leaves the atomic network, and the atom becomes ionized. The X-ray photon is deflected, weakened, and scattered. This effect most likely occurs with an electron on the outermost shell. When the density of a material or organ increases, the probability of occurrence of one of these two X-ray interactions also increases. Therefore, brightness levels on the X-ray image reflect the different densities of tissue. More strongly X-ray attenuating, or dense, tissues are displayed brighter on the image, whereas weakly attenuating tissues appear darker.
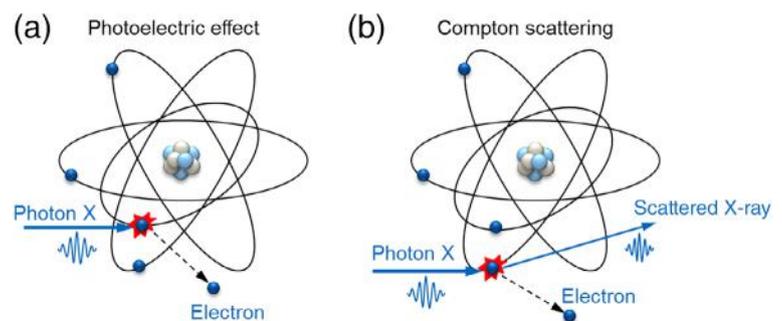

FIGURE 1 Schematic depictions of (a) the photoelectric effect and (b) Compton scattering

Finally, the detector records certain characteristics of the X-ray photons leaving the subject. Most detectors in medicine use a direct or indirect process. Indirect, solid-state detectors convert the incoming X-ray radiation with a scintillator into visible light, which is integrated with a photodiode. Instead of the scintillator and the photodiode, direct detectors use only an X-ray-sensitive semiconductor that generates charges when photons arrive (Taguchi, 2017), which are then detected by electrodes. The amount of charge of a pixel is proportional to the incident X-ray photon energy.

2.3 | Conventional X-ray imaging

Different clinical indications determine the design of an X-ray system. For example, mammography is the specific X-ray examination of the breast. With particularly "soft," low-energy X-ray radiation typically in the range of 25–40 kV (Russo, 2018), the glandular structures of the breast are displayed. In principle, the X-rays are generated in similar fashion as in conventional radiography. However, to ensure highest diagnostic quality and lowest radiation exposure, mammography has several additional technical features as follows: the use of molybdenum or molybdenum-rhodium anodes to generate a soft X-ray spectra; utilization of the Heel effect to image the tissue-tight chest wall for a higher dose rate; and use of a small focal spot to ensure the necessary high spatial resolution (Lewin, 2008). Mammography has extended in recent years to include a tomographic procedure called tomosynthesis. The mammography detector moves between 15° and 50° and acquires projection images. After reconstruction, slices of the breast may allow for a sharper image of glandular tissue, while the areas above and below appear out of focus (Skaane et al., 2013).

CT offers the next level in information content as a full tomographic modality, which is typically operated at an energy range of 80–140 kV. During the last four decades, CT has experienced explosive growth, which can be attributed to its short acquisition time, wide availability, and groundbreaking diagnostic benefits. In fact, the number of CT exams performed each year has significantly increased from ~21 million in 1995 to 88 million in 2018 in the United States alone (OECD, 2020). Over the last decade, a great effort has been made to develop advanced reconstruction algorithms to improve diagnostic quality and reduce radiation exposure (Hara et al., 2009; Noël et al., 2013; Prakash et al., 2010; Willemink & Noël, 2019). Marked technological advancements have also been made in the design of the gantry—a rotating ring-shaped frame in which an X-ray tube and detector are mounted on opposite sides. As the gantry rotates the X-ray tube and detector around the patient, X-rays are generated, attenuated by the patient, and recorded. Several thousand sectional views of the patient's body are acquired per rotation and cross-sectional images are reconstructed. From the resulting CT slices, 3D images and views can be generated from different angles. The resulting gray levels are described in Hounsfield units (HU), which make CT a quantitative and highly reproducible diagnostic modality. By definition, air has a value of −1,000 HU (black) and water a value of 0 HU. The HU values for body tissues depend on the system specifications and settings, but soft tissues are typically about 40–80 HU and bones about 1,000–1,500 HU (white) depending on their condition.

2.4 | New X-ray imaging technologies

Diagnostic CT is currently based on simple gray values (HU) representing anatomy and pathology on a larger scale. While anatomical information alone has been beneficial for clinical diagnostics, conventional CT integrates all detected signals into a single attenuation signal, which offers little functional information about the physiological state (e.g., on a biomolecular level) of an organ or region-of-interest. Nevertheless, improvements are within sight with the introduction of multi-energy CT (McCollough, Leng, Yu, & Fletcher, 2015). Dual-energy CT (DECT), a first step in the introduction of multi-energy CT, has already achieved status as an established clinical tool (Krauss & McCollough, 2019; Lohofer et al., 2018; Schmid-Bindert et al., 2012). Various approaches to acquire dual-energy data, such as dual-source CT (DSCT), rapid kVp switching CT (KVSCT), and dual-layer CT (DLCT), have recently been established (Ehn et al., 2018; Pelgrim et al., 2017; Sauter et al., 2018). DSCT scanners are equipped with two X-ray tubes as well as two detectors (Flohr et al., 2006; Johnson et al., 2006), while KVSCT systems use only a single tube-detector pair but involves an X-ray tube that can switch between two tube voltages in quick succession (Pinho, Kulkarni, Krishnaraj, Kalva, & Sahani, 2013). Moreover, DLCT can provide similar information by using two predefined detector layers to separate the X-ray photons into low- and high-energy bins (Postma, Das, Stadler, & Wildberger, 2015). With multi-energy CT, one can gain information about the elemental composition of an object by measuring the energy-dependent material-specific X-ray attenuation in three or more distinct energy regimes. Those measurements reflect changes in

Compton scattering and photoelectric effects as a result of material interactions with photons of different energies (Figure 2a). Furthermore, when the energy of the X-ray photons reaches the K-edge of an element, the excitation of K-shell electrons leads to a sudden increase in photon absorption. K-edge imaging is essential for the introduction of novel nanoparticle-based CT contrast agents (Roessl & Proksa, 2007; Schlomka et al., 2008; Si-Mohamed et al., 2018; G. Zhang, Naha, Gautam, Cormode, & Chan, 2018). By means of material decomposition (Alvarez & Macovski, 1976; Clark & Badea, 2014; Ehn et al., 2017; Maass, Baer, & Kachelriess, 2009; O'Donnell et al., 2017; Zimmerman & Schmidt, 2015), attenuation measurements can be used to distinguish between different materials (i.e., tissues and contrast agents) and quantify the elements in a single CT scan (Figure 2b). A novel nanoparticle-based multi-energy CT contrast agent should have a K-edge energy that is situated in a region of high photon flux (Figure 2c), therefore elements with
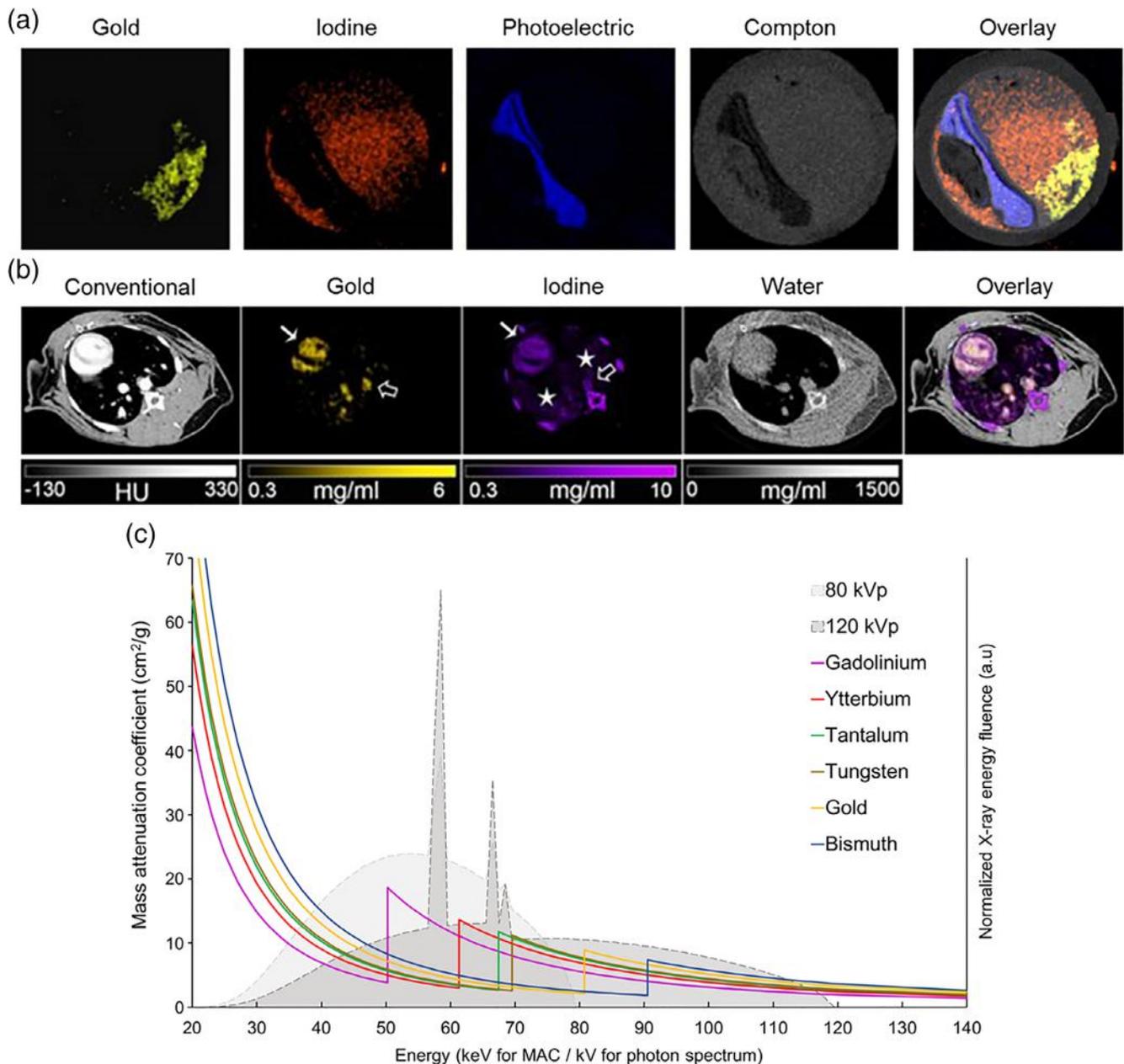

FIGURE 2 (a) Spectral CT images of gold, iodine, the photoelectric effect, and Compton scattering of an artery phantom. (b) Conventional CT image compared to SPCCT images of gold, iodine, and water of the chest of a rabbit injected with AuNP followed by iodine. (c) Mass attenuation coefficients of various heavy metal elements and X-ray photon energy spectra at tube voltages of 80 and 120 kV (Reprinted with permission from Cormode et al. (2010, 2017) and Kim et al. (2019)). CT, computed tomography; SPCCT, spectral photon-counting CT

K-edges between 50 keV ($Z = 64$; gadolinium) and 90 keV ($Z = 83$; bismuth) could be utilized (Carrascosa et al., 2010; Rabin, Manuel Perez, Grimm, Wojtkiewicz, & Weissleder, 2006). Of note, elements similar in atomic number to ytterbium (e.g., hafnium and tantalum) should produce most optimal contrast for these types of imaging techniques (J. Kim et al., 2018; Nowak, Hupfer, Brauweiler, Eisa, & Kalender, 2011; Roessler et al., 2016).

The introduction of photon-counting detectors (PCD) into the clinical setting can be seen as an opportunity to enable K-edge imaging (Muenzel et al., 2017; Pourmorteza et al., 2016; Si-Mohamed et al., 2017; Willemink, Persson, Pourmorteza, Pelc, & Fleischmann, 2018). First, with the capability of counting individual X-ray photons while rejecting noise, this unique technology has the potential to achieve a near-ideal signal-to-noise ratio for a given X-ray dose, making it possible to obtain high-quality spectral data with a factor of two or more in radiation reduction. Second, PCD can perform spectral detection by discriminating the energy of individual photons via pulse height analysis and dividing them into more than the two energy bins used in current DECT systems. Third, PCD have significantly improved spatial resolution, which allows visualization of small structures (e.g., contrast-enhanced vessels) and reduction of artifacts, such as blooming and beam hardening.

A similar development toward spectral or multi-energy X-ray imaging has seen attraction in mammography as a promising clinical tool (Carton, Ullberg, & Maidment, 2010). K-edge imaging is also used in contrast-enhanced dual-energy X-ray breast imaging, or DEM. The low- and high-energy spectra are placed below and above the K-edge of the contrast agent, respectively. The low-energy images provide soft tissue contrast while high-energy images above the K-edge contain substantial information from the agent. A weighted dual-energy subtraction is then done to suppress background variations and enhance the signal from the contrast agent, while providing anatomical data of diagnostic quality. DEM is currently performed with iodinated agents and initial studies have illustrated that the availability of iodine images can significantly improve the detection and depiction of lesions in dense breasts (Carton et al., 2010). Clinical data indicates that the sensitivity of DEM is superior to conventional mammography and matches that of contrast-enhanced breast MRI (S. C. Chen et al., 2007; Diekmann et al., 2011; Dromain et al., 2012).

Elements with Z ranging from 42 (molybdenum) to 52 (tellurium) are better suited for the energies used in DEM (26–49 kV) than iodine (Karunamuni & Maidment, 2014). The lower K-edge energies (20–32 keV) allow for greater flexibility in the positioning of the high-energy spectrum, resulting in optimal dual-energy subtraction. Novel nanoparticle agents based on silver ($Z = 47$) have recently been shown to produce strong DEM contrast (Hsu et al., 2018; Karunamuni et al., 2016). Silver is also suited for spectral imaging with photon-counting mammography (Lau, Hsu, Cederström, Cormode, & Maidment, 2019), where considerable reduction in radiation dose can be achieved (E. B. Cole, Toledano, Lundqvist, & Pisano, 2012). The system is equipped with PCD that can discriminate detected photons using two different energy thresholds and extract information about material compositions, such as breast density. However, there is room for further investigations with this technology; with topics such as alternative energy binning methods remaining unexplored.

3 | X-RAY CONTRAST AGENTS

3.1 | Small molecules and heavy metal complexes

Poor native contrast between different soft tissues has prompted the use of exogenous contrast agents since the early development of X-ray imaging technologies. The clinically approved X-ray contrast agents are barium sulfate suspensions, which are mostly used for GI tract imaging, and iodinated small molecules, which are mainly used in many oral and intravascular applications. Iodine-based contrast agents were initially developed as ionic, mono-iodinated molecules, such as sodium iodide, and have since evolved to nonionic, tri-iodinated derivatives of benzoic acid, such as iohexol (De La Vega & Hafeli, 2015). The current formulations provide excellent water solubility, improved biological tolerance, and low osmolality. Despite the efforts made to optimize the physicochemical properties of these agents, further improvement is still needed given that they have very short blood circulation times and generate limited contrast due to low payloads (Dean et al., 1983). They are also nonspecific, which leads to random vascular permeation and very low tumor accumulation. Moreover, their rapid clearance via the kidneys can induce nephrotoxicity in those with renal disease (Tepel et al., 2006) and they are known to cause adverse reactions in some patients (Bottinor, Polkampally, & Jovin, 2013). To overcome these limitations, a range of elements and a variety of formulations have been proposed as potential alternative X-ray contrast agents. Earlier reports to develop new X-ray diagnostic agents focused on systems such as tungsten clusters or gadolinium chelates (Schmitz, Wagner, Schuhmann-Giampieri, Krause, & Wolf, 1997;

S. Yu et al., 2000). The number of metal chelates and metalloclusters formed from different electron-dense elements, such as hafnium and tantalum, has greatly expanded since then, and their physical characteristics, biocompatibility, and contrast properties have been studied (Berger et al., 2017). A more extensive discussion of these older heavy metal complexes can be found in a review article by S. B. Yu and Watson (1999). However, none of the chelates or cluster compounds has been approved for X-ray imaging so far.

3.2 | Metal-based nanoparticles

Much of the research on novel X-ray contrast agents in recent decades has been devoted to nanoparticle formulations. Given the low sensitivity of X-ray imaging, these nanoparticle agents typically contain a dense core loaded with hundreds to millions of contrast generating atoms and are coated by silica, proteins, polymers, lipids, or other compounds that yield desired pharmacological and physicochemical properties. Compared to small molecules, nanoparticles have higher payloads per entity, thus may prove more compatible with patients whose kidney function is impaired, as fewer excretion events would be needed (Chakravarty, Unold, Shuboni-Mulligan, Blanco-Fernandez, & Shapiro, 2016; Hsu et al., 2019; Mukundan et al., 2006). The most frequently reported nanoparticle types for X-ray imaging are lipid-based structures (e.g., liposomes, emulsions, lipoproteins, or micelles), solid core-based (e.g., metal, metal alloy, or metal salt), or combinations of the two. For metal core-based nanoparticles, gold ($Z = 79$) has been extensively studied since it has a high K-edge energy of 80.7 keV, is very dense (19.3 g/cm^3) and is generally regarded as biocompatible and bioinert. In addition, AuNP are well developed in terms of synthetic control over their size, shape, and surface chemistry (Bouché et al., 2020; L. E. Cole, Ross, Tilley, Vargo-Gogola, & Roeder, 2015). An increasing number of studies have featured other elements that also have a high K-edge energy, such as lanthanides, bismuth, tantalum, tungsten, and platinum (De La Vega & Hafeli, 2015). As mentioned in previous sections, nanoparticles based on these elements are well-suited as CT contrast agents as their K-edges fall within the diagnostic energy range employed by many clinical CT imaging scanners. In fact, there are a large number of reports supporting their use as contrast agents for imaging applications with various CT modalities (Cormode et al., 2014). On the other hand, X-ray mammography utilizes much lower tube energies than CT and would therefore benefit from nanoparticle agents based on elements with lower atomic numbers such as silver, which have lower K-edge energies than iodine (Karunamuni et al., 2016).

Nanoparticles are very small structures that range between 1 and 1,000 nm in size. Some X-ray nanoparticle contrast agents have been designed to be in the ultrasmall size range (<5 nm) to allow rapid clearance from the body, which is an essential criterion for clinical approval (C. Zhou, Long, Qin, Sun, & Zheng, 2011). Those that are larger in size and possess desired surface coatings have been utilized as blood pool contrast agents since they are cleared from circulation at a slower rate (Naha et al., 2016). They can also be used as contrast agents for disease imaging via both passive and active targeting (Hsu et al., 2018; Toy, Bauer, Hoimes, Ghaghada, & Karathanasis, 2014). Their physico-chemical properties can be fine-tuned to encourage uptake by certain cell types, thereby enabling cell-based therapies and tracking via X-ray imaging (J. Kim, Chhour, et al., 2017). In addition, most reported nanoparticles are approximately spherical, but they can be formed into other shapes, such as cages, stars, or rods, which can greatly influence their pharmacokinetics, optical properties, and suitability for other imaging applications (Hajfathalian et al., 2018; J. Li et al., 2015). Furthermore, nanoparticle X-ray agents can frequently offer both diagnostic and therapeutic properties concurrently (Al Zaki et al., 2014; Curry, Kopelman, Shilo, & Popovtzer, 2014). Most importantly, these nanoparticle agents, having novel chemical compositions, can produce strong contrast for advanced forms of X-ray imaging modalities, such as SPCCT and DEM (Karunamuni et al., 2014; J. Kim et al., 2018).

3.2.1 | Rapidly cleared X-ray agents

Many preclinical studies have supported the relevance of heavy metal-based nanoparticles for X-ray imaging applications; however, sufficient (if not complete) clearance from the body is required for their eventual clinical translation due to the inability of the human body to metabolize or transport these elements. Rapid renal excretion should minimize uptake by organs of the reticuloendothelial system (RES), thereby avoiding prolonged body retention and possible safety concerns. Urinary clearance is mainly carried out by glomerular filtration in the kidneys. Found in the renal corpuscle of a nephron, or the basic functional unit of the kidneys, the glomerulus (Figure 3a) is a network of capillaries enclosed by the Bowman's capsule (Scott & Quaggin, 2015). The glomerular capillaries are lined by a monolayer of

glycocalyx-coated endothelial cells with fenestrations of 70–90 nm in diameter. This endothelium is supported by the glomerular basement membrane (GBM) that has a net polyanionic charge and contains 2–8 nm pores. The distal layer of the GBM is composed of visceral epithelial cells, or podocytes, with foot processes that form narrow and uniform filtration slits of 4–11 nm in width. The surface of this layer is also covered by negatively charged glycoproteins. Together, these three layers with distinctive pore sizes and negatively charged surfaces make up the glomerular filtration barrier (Figure 3b) (Menon, Chuang, & He, 2012). Therefore, renal clearance of nanoparticles relies on a highly selective sieve that is mostly dependent on size and surface charge among other factors (Du, Yu, & Zheng, 2018; J. Wang & Liu, 2018).

Particle size plays a major role in the process of glomerular filtration. A filtration-size threshold of 5.5 nm in hydrodynamic diameter (D_h) has been established for nanoparticles, which is similar to that of molecules and proteins (Choi et al., 2007). D_h is referred to the diameter calculated from the dynamic diffusional properties of a particle within a fluid medium, which is influenced by the hydration layer formed around the coating or surface modifications of the particle (Maguire, Rosslein, Wick, & Prina-Mello, 2018). It is generally larger than the internal core size of the particle. Renal excretion of X-ray nanoparticle agents was first demonstrated by Hainfeld, Slatkin, Focella, and Smilowitz (2006) using AuNP of 1.9 nm in core diameter (the D_h of the AuNP was not reported in this study). The nanoparticles were swiftly excreted through the renal system as evidenced by high contrast enhancement in the kidneys and bladder in
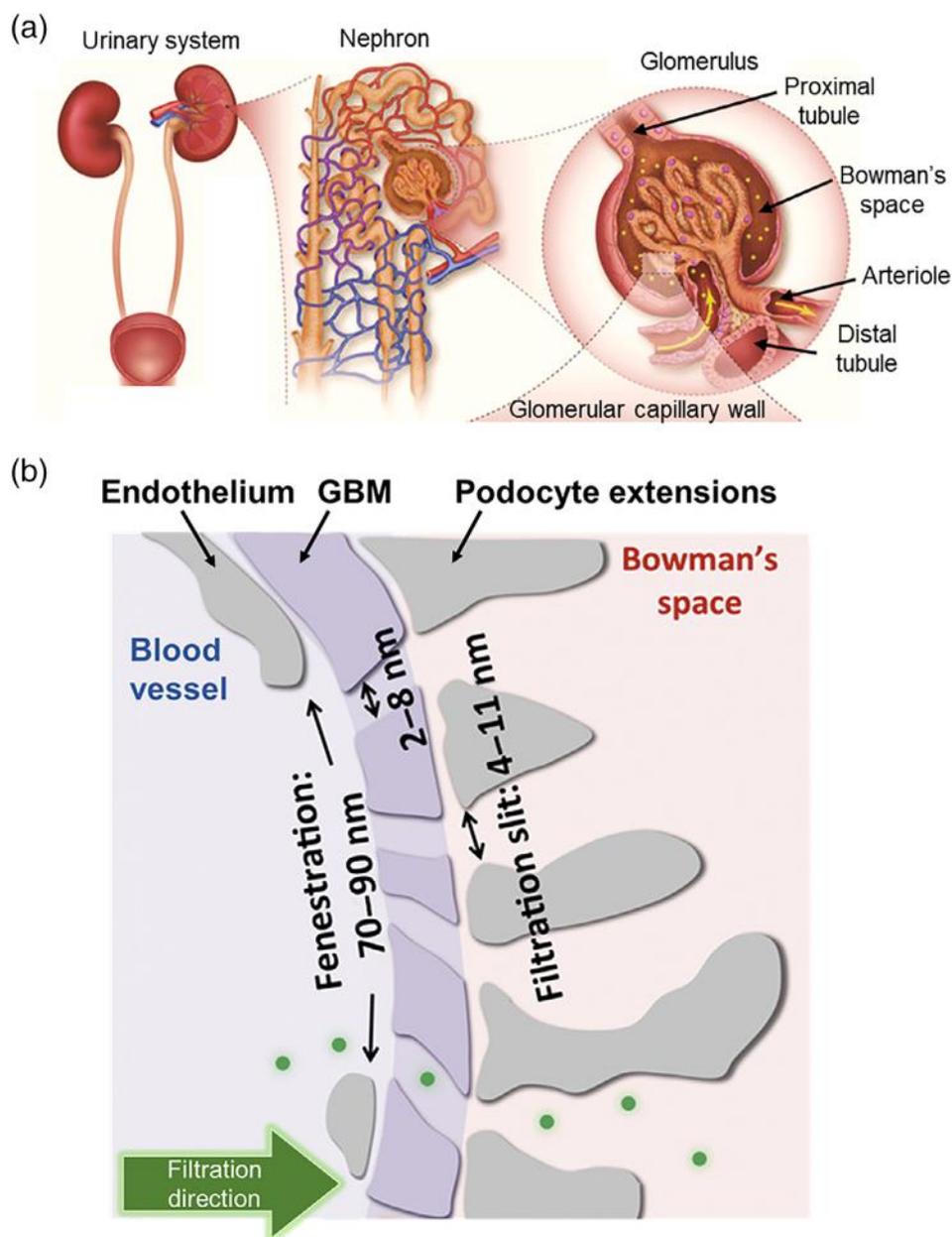

FIGURE 3 (a) Diagram of the urinary system with a detailed view of the kidney including components of nephron and glomerulus. (b) Schematic depiction of the three distinctive layers of the glomerular filtration barrier (Reprinted with permission from J. Liu, Yu, Zhou, and Zheng (2013) and Wang and Liu (2018))

postinjection X-ray images. Following this initial report, subsequent studies have shown that up to 50% of the injected dose (ID) can be excreted renally for AuNP with $D_h < 6$ nm at 24 hr postinjection (Du et al., 2017; Xu et al., 2017; C. Zhou et al., 2011). It was found that renal clearance efficiency of nanoparticles generally decreased with increasing size, while those much larger in size ($D_h > 10$ nm) were mainly taken up in the RES organs.

Renal clearance of nanoparticle CT contrast agents based on other heavy elements, particularly bismuth (Brown & Goforth, 2012; L. Dong, Zhang, et al., 2019; Naha et al., 2014) and tantalum (Bonitatibus, Torres, Goddard, FitzGerald, & Kulkarni, 2010; Bonitatibus et al., 2012; FitzGerald et al., 2016), has also been evaluated. Interestingly, bismuth can degrade into molecular Bi^{3+} species in vivo as a result of oxidative instability, thus allowing several bismuth nanoparticle formulations with $D_h > 5.5$ nm to undergo kidney filtration (Brown & Goforth, 2012). Furthermore, FitzGerald et al. (2016) developed tantalum oxide nanoparticles with a D_h of 3.1 nm that have a good safety profile and can be cleared renally with high efficiency. They found that >98% of ID was excreted from the body within 48 hr after injection, which is among the best clearance of all nanoparticle agents reported to date. More recently, Hsu et al. (2019) reported similar renal clearance efficiency (85% of ID at 24 hr after injection) using a 3.1 nm silver sulfide nanoparticle formulation that can provide both DEM and CT contrast (Figure 4a). This study demonstrated that nanoparticles of this core size can circulate longer than iodine agents, resulting in strong vascular contrast (Figure 4b). In comparison to similar, but larger nanoparticles, their rapid clearance via urine has yielded minimal retention in the RES organs (Figure 4c). These results clearly indicate that renal filtration efficiency and tissue retention of nanoparticle agents are heavily influenced by their size.

The clearance properties are also affected by particle's surface charge, as well as shape and core composition. Recent studies investigating the effect of surface charge on glomerular filtration have shown that nanoparticles with low molecular weight zwitterionic or neutral coatings, such as glutathione, undergo more rapid and efficient renal excretion than those with single-charged surface ligands (FitzGerald et al., 2016; C. Zhou et al., 2011). Zwitterionic ligands can minimize the adsorption of serum proteins on the nanoparticle surface, thereby maintaining a small overall size for
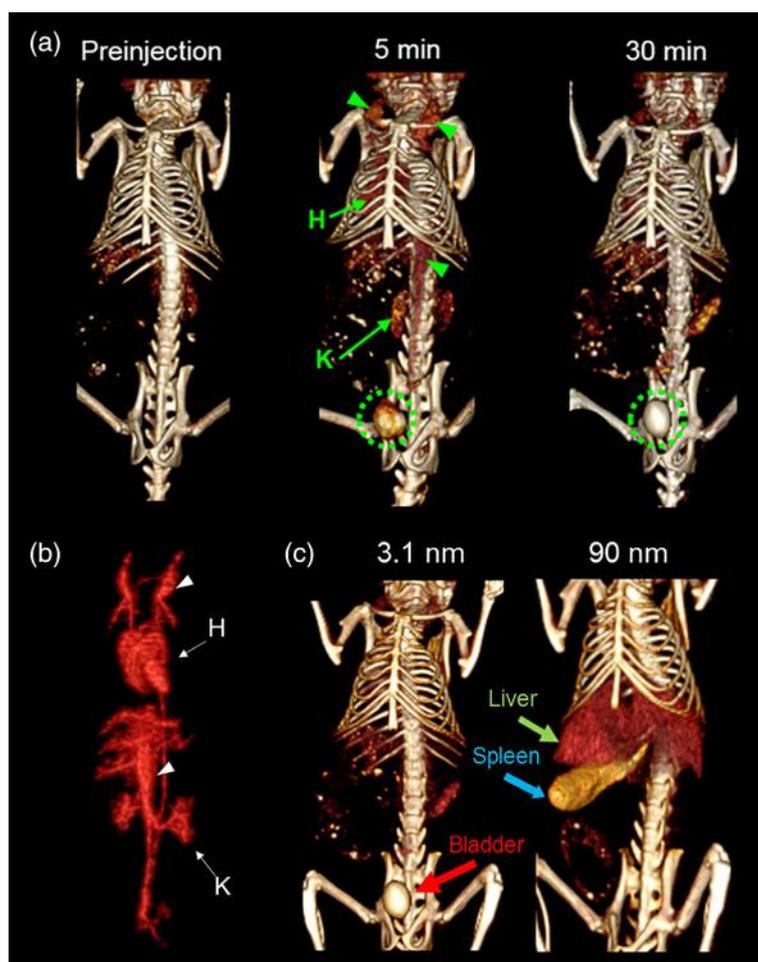

FIGURE 4 (a) CT images of a mouse injected with 3.1 nm silver sulfide nanoparticles. (b) Segmentation data to visualize vascular contrast and kidney filtration of the same mouse immediately postinjection. (c) CT images of mice injected with small- and large-sized silver sulfide nanoparticles at 2 hr postinjection (Reprinted with permission from Hsu et al. (2019)). CT, computed tomography

optimal renal filterability. Of note, surface charge has greater influence on the filtration of nanoparticles within the 6–8 nm size range, whereas size is the key determinant in the renal clearance of particles with $D_h < 6$ nm. Furthermore, nanoparticle X-ray agents in other shape variations, such as stars (D. Tang, Gao, Yuan, Guo, & Mei, 2017) and tubes (Hu et al., 2018), can also be excreted via urine, although less is known about the renal clearance mechanisms of nonspherical nanoparticles. More recently, using an array of similarly sized nanoparticles with different core compositions (i.e., varying ratios of gold and silver), S. Tang et al. (2016) found that renal clearance efficiency was inversely related to the core density as a result of density-dependent margination in laminar blood flow.

Rapidly cleared nanoparticle X-ray contrast agents have been developed to reduce tissue retention and increase their chance for clinical translation. However, due to their small size, these nanoparticles sacrifice some relevant properties for certain imaging applications, such as long circulation times, effective targeting, and accumulation in tumors, which would be achievable by nanoparticles larger than 5 nm. Nevertheless, we expect to see more progress made in engineering of sub-5 nm nanoparticle X-ray agents with other heavy elements and novel surface coating ligands. Further quantitative investigation should be done to better understand the dependency of nanoparticle charge on renal filtration as there are several reports with contradictory findings.

3.2.2 | Long circulating agents

Nanoparticles that circulate for a long time have advantages over rapidly cleared agents (e.g., iodinated small molecules) since they provide longer lasting contrast and have greater opportunity to enter disease sites. Long circulating agents are especially useful for imaging changes in vascularity such as sustained angiogenesis and permeable vasculature, which are known hallmarks of cancer. The leaky nature of tumor neovessels allows agents to passively accumulate in the diseased tissues through the enhanced permeability and retention (EPR) effect, enhancing contrast for better tumor detection (Sykes, Chen, Zheng, & Chan, 2014). Thus, many efforts, such as adjusting nanoparticle size and surface coating, have been made to synthesize agents with favorable pharmacological properties that help to increase blood circulation times.

Nanoparticles with D_h larger than the filtration-size cutoff can remain in circulation for a longer time due to the lack of transport across the glomerular filtration barrier (Choi et al., 2007). Furthermore, the surfaces of these nanoparticles are often modified with hydrophilic polymers, such as poly(ethylene glycol) (PEG), to prolong blood retention time as this ligand type can prevent aggregation and opsonization, which leads to uptake by the RES organs (Huo et al., 2017; Suk, Xu, Kim, Hanes, & Ensign, 2016). The long polymer chains also significantly increase the overall size of the agents, allowing them to bypass kidney filtration and renal clearance (L. E. Cole, McGinnity, Irimata, Vargo-Gogola, & Roeder, 2018; Hussain et al., 2019). Thus, the combination of increased nanoparticle size and modified surfaces gives way to long circulating agents.

Cormode et al. (2017) synthesized PEGylated AuNP that was 18 nm in D_h for in vivo imaging of rabbits using SPCCT. With this imaging system, they were able to distinguish the contrast between AuNP and an iodinated molecular agent in the heart. AuNP were observed to remain in the blood pool throughout the entire study (i.e., 41 min) while contrast from iodine decreased over time. Indeed, such AuNP have previously been reported to circulate for several hours (Cai et al., 2007). Interestingly, Naha et al. (2016) developed an array of thiol-PEG capped gold silver alloy nanoparticles (GSAN) with a D_h of 16 nm. Silver produces excellent DEM contrast while the inclusion of gold provides CT contrast and improves overall biocompatibility, making GSAN a dual-modality X-ray contrast agent (Karunamuni et al., 2014). Following the administration of GSAN to a murine model of breast cancer, CT imaging revealed significant contrast in the heart and blood vessels (Figure 5a) and also at the tumor site (Figure 5b), indicating the passive tumor targeting capability of GSAN via the EPR effect. DEM imaging studies also showed that GSAN could provide strong blood pool contrast (Figure 5c) and higher contrast in breast tumors compared to iopamidol (Figure 5d). Other examples of long circulating agents with large size and PEG coating include 120 nm nanoemulsions of iodinated oil for blood pool imaging with micro-CT (Hallouard et al., 2011), 100 nm iodinated liposomes for imaging small blood vessels with micro-CT (Mukundan et al., 2006), and 30 nm AuNP for imaging primary lung cancer with dual-energy micro-CT (Ashton et al., 2014).

Nanoparticles have also been modified with other hydrophilic polymers to achieve long circulation times (Kodiyan, Silva, Kim, Aizenberg, & Mooney, 2012). For example, AuNP coated with polyethyleneimine had a circulation half-life close to 8 hr and were used to image lymph nodes via CT (Y. Zhang et al., 2016). Renally clearable AuNP and other X-ray contrasting nanoparticle types can be encapsulated in larger, biodegradable polyphosphazene (PCPP) polymeric

nanospheres to increase both CT contrast generation and blood circulation time and subsequently break down into harmless byproducts for swift clearance (Cheheltani et al., 2016; Chhour et al., 2014; J. Kim et al., 2019). Furthermore, the use of biomimetic coatings, such as cell membranes and bovine serum albumin (BSA), can minimize the uptake of nanoparticles by phagocytic cells, thus improving their blood residence time (Jin et al., 2015; Piao et al., 2014; You et al., 2017).

In addition to cancer imaging applications, several long circulating X-ray agents have been developed to study atherosclerosis. Notably, CT is preferable to alternative methods such as MRI for imaging such disease in the clinical
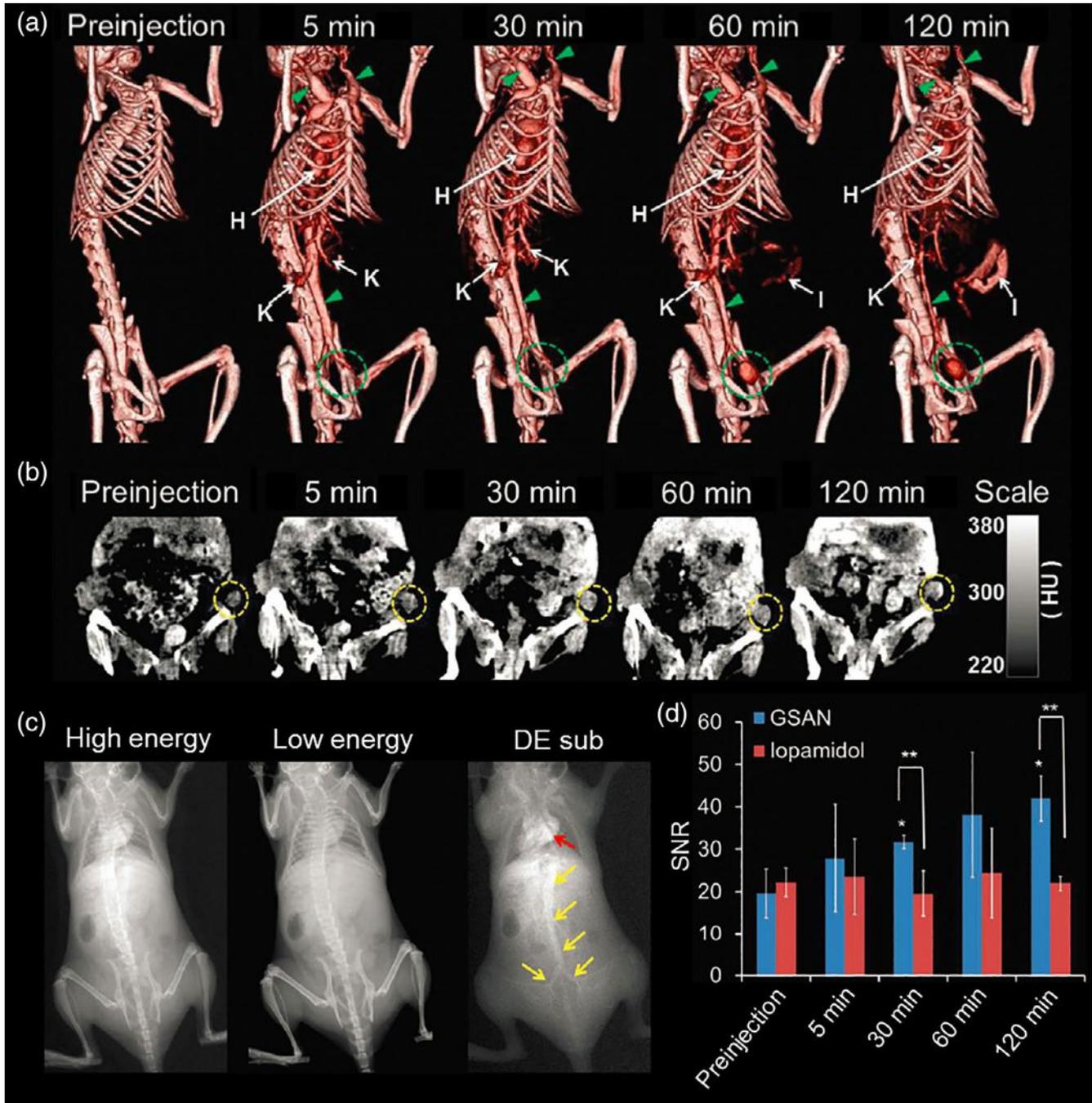

FIGURE 5 CT images of a mouse injected with GSAN showing contrast enhancement in the (a) blood pool and (b) breast tumors. (c) DEM images of a mouse injected with GSAN showing vascular contrast. (d) Quantification of DEM contrast in the tumors compared to an iodinated agent (Reprinted with permission from Naha et al. (2016)). CT, computed tomography; DEM, dual-energy mammography; GSAN, gold silver alloy nanoparticles

setting due to its high performance in regions of the body where there is a lot of motion, such as the heart. For example, Ye et al. (2014) showed that dendrimer-entrapped AuNP with PEG coating could circulate up to 6 hr, which proved to be beneficial for CT imaging of murine macrophages in an apolipoprotein-E-gene-deficient mouse model. Other novel formulations for detecting macrophage content of atherosclerotic plaque via CT include iodine-based polymeric nanoparticles and nanoemulsions (Ding et al., 2013; Hyafil et al., 2007).

Although long circulating agents have great advantages in vascular imaging and subsequent disease detections, these contrast agents tend to accumulate in the liver and spleen. Significant accumulation of some heavy metal elements in the RES organs can lead to potential long-term toxicity, such as liver fibrosis or cirrhosis, as was observed in patients that had been administered Thorotrast, a thorium dioxide nanoparticle used in the 20th century (Selinger & Koff, 1975). Moreover, the current concerns over the retention of gadolinium in patients injected with gadolinium chelates, underscore the challenges that an agent that is partially retained would face for FDA approval (Levine, McDonald, & Kressel, 2018; McDonald et al., 2015). Thus, methods to optimize clearance characteristics while retaining long circulation times should be further explored.

3.2.3 | Theranostic X-ray agents

Nanoparticle agents that have both therapeutic and diagnostic functions in a single platform are known as theranostics (X. Chen, Song, Chen, & Yang, 2019). This has the advantage that the disease site can be visualized and also that knowledge of the distribution of the theranostic agent can be used in disease planning. Many X-ray contrasting nanoparticles possess intrinsic therapeutic properties, such as for photothermal therapy (PTT) or radiotherapy (RT), and/or additional imaging functionalities, such as photoacoustic imaging (PAI), including certain agents based on silver (Cui et al., 2017), gold (Curry et al., 2014; Hajfathalian et al., 2018; Jing et al., 2014), tungsten (Cheng et al., 2014; Z. Zhou et al., 2014), hafnium oxide (Bonvalot et al., 2017), and bismuth (Z. Li et al., 2017; J. Liu et al., 2015; Yang et al., 2018). PTT involves the use of a photosensitizer to convert NIR light into heat for localized tissue ablation. A recent study by Lei et al. (2017) demonstrated the use of sub-5 nm polyvinylpyrollidone-coated bismuth nanodots as a potential theranostic agent for tumor imaging with CT and precise cancer treatment with PTT. CT imaging was used to locate bismuth nanodots in the mice bearing tumors and to guide laser irradiation needed for PTT. In an interesting example, breast tumor-bearing mice were injected with 3 nm rhenium disulfide nanoparticles and imaged using a dual-source spectral CT scanner under different tube voltages (X. Wang et al., 2019). Contrast in the tumors was significantly enhanced by the nanoparticles at any given X-ray energy while the signals in surrounding tissues as well as tumors injected with an iodinated agent were largely reduced at higher energies. Moreover, tumors treated with the nanoparticles were completely eliminated after PTT was performed on them.

Several high Z elements, specifically those that provide strong contrast in CT, can also achieve radiosensitization due to the large X-ray attenuation coefficients, resulting in the release of photoelectrons and free radicals upon X-ray absorption which enhances radiation-induced DNA damage (Al Zaki et al., 2014; Dou et al., 2016; Hazkani et al., 2017; Her, Jaffray, & Allen, 2017). McQuade et al. (2015) demonstrated that biodegradable polymeric micelles loaded with AuNP and iron oxide nanoparticles could be used as a contrast agent for both CT and T_2-weighted MR imaging to better delineate tumor margins and assist with RT treatment planning. When combined with RT, this theranostic agent resulted in extensive cellular DNA damage in vitro and improved the mean survival and tumor responses of tumor-bearing mice. In addition, RT can be further combined with PTT to realize synergistic therapeutic effects and improve treatment efficacy (Mao et al., 2016; Y. Wang et al., 2016; Wen et al., 2016; Yong et al., 2015). For example, 40 nm bismuth nanoparticles coated with PEGylated phospholipids were injected into breast tumor-bearing mice (N. Yu et al., 2018). These nanoparticles can passively accumulate in the tumor region, allowing for tumor imaging with CT as well as image guided thermoradiotherapy. The synergistic effects resulted from the combination of RT and PTT induced greater antitumor efficacy than that of a single treatment alone.

In recent years, X-ray contrasting nanoparticles have received growing interest for use as carriers for nucleic acids and therapeutics, such as siRNA and chemotherapy drugs, to mitigate the shortcomings of conventional drug delivery systems. For example, a polymer-AuNP complex was developed as a gene-chemical co-delivery vehicle to treat dopaminergic neuron degeneration and allow drug delivery tracking via CT imaging in a murine model of Parkinson's disease (L. Liu et al., 2019). Upon entering specific diseased cells, the complex was degraded in the reactive oxygen species (ROS) rich microenvironment, releasing siRNA and curcumin for downregulation of α-synucelin gene (SNCA) and inhibition of SNCA aggregation. The synergistic therapy resulted in the recovery of neurons and motor performance of

the mice. Simultaneously, the released AuNP would aggregate to form gold clusters, and could thus be detected with CT. Moreover, nanoparticles can be designed to respond to specific external and/or internal stimuli, such as NIR light, magnetic field, acidic pH, and hypoxia, for triggered drug release at targeted sites with controllable therapeutic outcome (Jin et al., 2017; W. Lin et al., 2017; Tian et al., 2014). Interestingly, Z. Li et al. (2018) developed such theranostic agent based on 120 nm largely porous bismuth nanostructures, known as nanoraspberries (Figure 6a), which were further stabilized by BSA. They found that this agent could load doxorubicin at high capacity, accumulate passively at the tumor site, and release the drug when exposed to NIR light irradiation and acidic pH conditions (Figure 6b). This agent also provided CT (Figure 6c) and PAI contrast in HeLa tumor-bearing mice and served as a PTT agent due to the afore-mentioned intrinsic theranostic properties of bismuth. Notably, all tumors were eliminated in mice treated with the agent in combination with PTT and triggered drug release (Figure 6d), demonstrating the superior therapeutic efficacy of combined therapies over either treatment alone.

Recent studies have reported remarkable advances in the development of theranostic nanoparticles that are both active for X-ray imaging and also provide therapeutic effects. We expect to see more reports on novel X-ray theranostic agents with elements other than gold and bismuth and also with a variety of shapes, hybridizations, and stimuli-responsive coatings for improved contrast generation and better therapeutic efficacy. Yet, a thorough evaluation of their long-term retention, biodegradation, and safety profiles is needed to increase their likelihood for clinical translation.
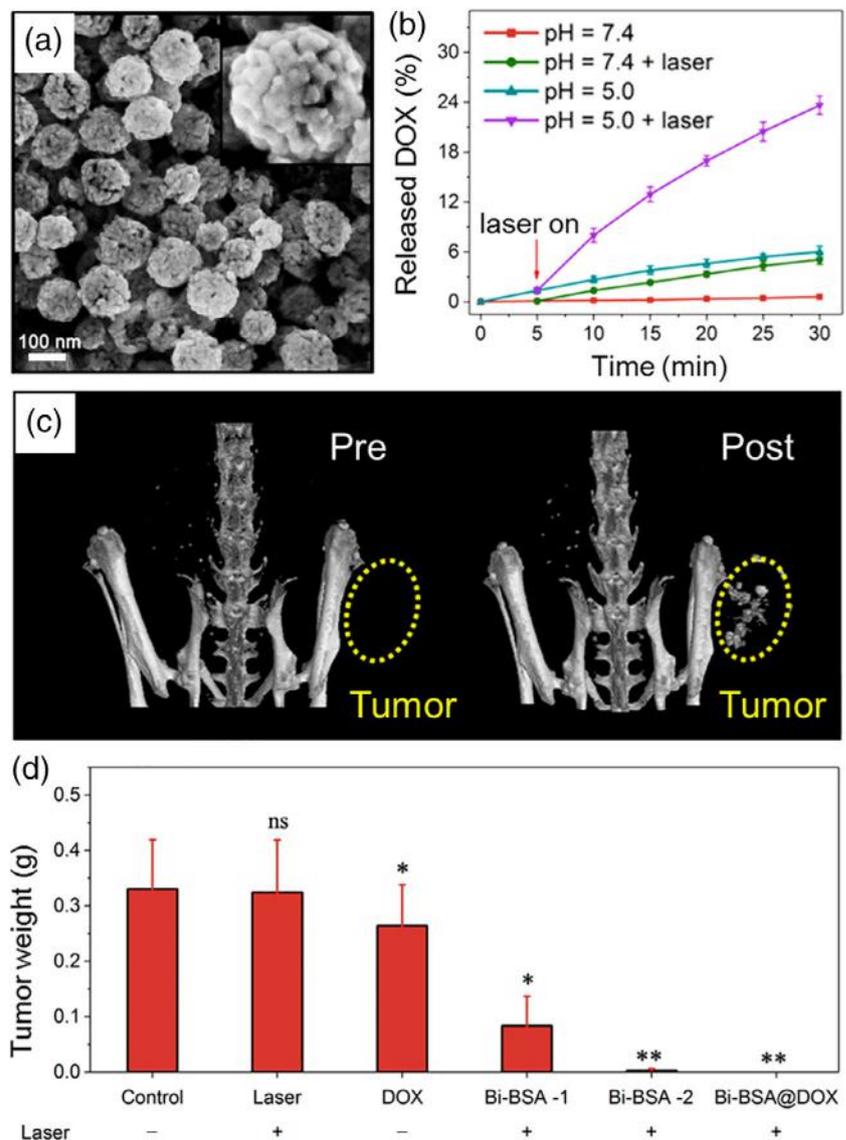

FIGURE 6 (a) SEM image of bismuth nanoraspberries. (b) DOX release profiles following exposure to different pH conditions with or without laser irradiation. (c) CT images of tumors acquired prior to and after injection of bismuth nanoraspberries. (d) Tumor weights of control and different treatment groups (Reprinted with permission from Li, Hu, et al. (2018)). CT, computed tomography; DOX, doxorubicin; SEM, scanning electron microscopy

3.2.4 | Targeted X-ray agents

Targeted imaging provides the opportunity to characterize diseases for factors such as their level of inflammation or cancer type (Toy et al., 2014). Agents with greater targeting selectivity have better delivery efficiency and improved diagnostic and therapeutic outcomes with minimal off-target effects. This can be achieved by conjugating the surface of X-ray contrast agents with targeting moieties that have specific binding affinity for certain cellular components or biomolecules (Yhee, Lee, & Kim, 2014). The challenge for X-ray imaging is that its sensitivity toward contrast media is quite low, therefore only highly expressed targets can be imaged (X. Li, Anton, Zuber, & Vandamme, 2014). Consequently, a large variety of targeting ligands, such as the PDL1 antibody (Meir et al., 2017), epidermal growth factor receptor antibody (Dreifuss et al., 2015; Reuveni, Motiei, Romman, Popovtzer, & Popovtzer, 2011), LyP-1 peptide (Laakkonen, Porkka, Hoffman, & Ruoslahti, 2002), hyaluronic acid (Jin et al., 2015), folic acid (Huang et al., 2011; Khademi et al., 2018; J. Lin et al., 2018), bisphosphonate (L. E. Cole, Vargo-Gogola, & Roeder, 2014, 2015), and insulin (Betzer et al., 2017; Shilo, Motiei, Hana, & Popovtzer, 2014), has been used in functionalizing X-ray nanoparticle contrast agents for targeted imaging of cancers, microcalcifications, and neurodegenerative disorders. For example, nanoparticle CT contrast agents based on gold (Hainfeld et al., 2011), platinum (Chou et al., 2010), or bismuth (L. Li et al., 2018) were conjugated with monoclonal antibodies, such as trastuzumab, to target abundantly expressed human epidermal growth factor receptor (HER2), which is useful in imaging and treating HER2 positive breast cancer.

Vascular markers, such as $\alpha_v\beta_3$ integrin receptor and vascular endothelial growth factor receptor, are also ideal targets for imaging cancer. The integrin $\alpha_v\beta_3$ contributes to angiogenesis and metastasis, and is highly expressed on endothelial cells within the neovasculature of several tumor types such as osteosarcoma (Lu et al., 2018). RGD (Arg-Gly-Asp) peptides are commonly used for targeting such receptors and for producing vascular-targeted X-ray contrasting nanoparticles (Zhu, Fu, Xiong, Shen, & Shi, 2015). A recent study by Ashton et al. (2018) investigated the impact of AuNP-augmented RT on tumor vascular permeability and subsequent effect on the delivery of nanoparticle therapeutics. RGD peptides were first conjugated to the surface of 25 nm AuNP and injected into mice with primary soft tissue sarcoma, which were treated with varying radiation doses. Iodinated liposomes were injected at 24 hr post irradiation and DECT imaging was performed to differentiate the signals of gold and iodine in the tumors and to quantify each separately (Figure 7a). Significant iodine accumulation was observed with RGD-functionalized AuNP compared to non-targeted AuNP and control (Figure 7b), particularly at lower radiation doses (5 Gy), indicating that vascular-targeted AuNP could deliver the radiation dose preferentially to endothelial cells, and thus, reduce the dose necessary for RT. The combination of targeted AuNP with 5 Gy RT greatly increased vascular permeability and further improved the delivery of liposomal doxorubicin to the tumors, which resulted in significant reduction in tumor growth (Figure 7c).

Besides targeting cancer related biomarkers, X-ray contrast agents have also been modified with fibrin targeting moieties to enable the imaging of thrombi (Pan et al., 2009). The occurrence of fibrin-rich thrombi in the arteries is usually the source of myocardial infarction, strokes, and pulmonary embolism. Interestingly, J. Y. Kim et al. (2015) coated AuNP with glycol-chitosan and further conjugated them with fibrin-binding peptides to allow in vivo detection and quantification of cerebral thromboembolism as well as carotid thrombosis using micro-CT. The information obtained by cerebral CT imaging was then used to guide thrombolytic therapy and optimize the dosing of tissue plasminogen activator, which is a drug known for treating blood clots. A similar strategy for micro-CT imaging of thrombus was pursued using silica-coated AuNP functionalized with thrombin-activatable fluorescent peptide (Kwon et al., 2018). Moreover, spectral or multicolor CT has been employed to further distinguish targeted heavy metal nanoparticles from soft tissues and calcified materials (Schirra et al., 2012). Pan et al. (2010) reported the first example of thrombus imaging with spectral CT using bismuth nanoparticles targeted with fibrin-specific antibodies. These nanoparticles greatly enhanced the contrast of fibrin clot surface, allowing the thrombus to be distinguished from highly attenuating plaque calcium deposits. A nanoparticle formulation based on ytterbium was also targeted to thrombi in the same manner to provide higher detection sensitivity in K-edge imaging than for bismuth (Pan et al., 2012). Furthermore, gold core high-density lipoprotein nanoparticles were shown to specifically target macrophage-rich plaques in atherosclerotic mice, and whose accumulation could be identified and be distinguished from nearby aorta with spectral CT imaging (Cormode et al., 2010). Calcifications in the plaque of these mice could also be discriminated using this imaging system.

A wide range of X-ray contrasting nanoparticles has been applied to several highly expressed targets, such as HER2, folate receptors, $\alpha_v\beta_3$ integrin receptors, and fibrins, to make disease imaging feasible with various forms of CT imaging technology. In the coming years, the first studies where targeted imaging is done using new X-ray imaging techniques such as DEM and photon-counting mammography will likely be reported. It may be possible to functionalize silver-based nanoparticles with bisphosphonate for contrast-enhanced, targeted imaging of microcalcifications in dense breast
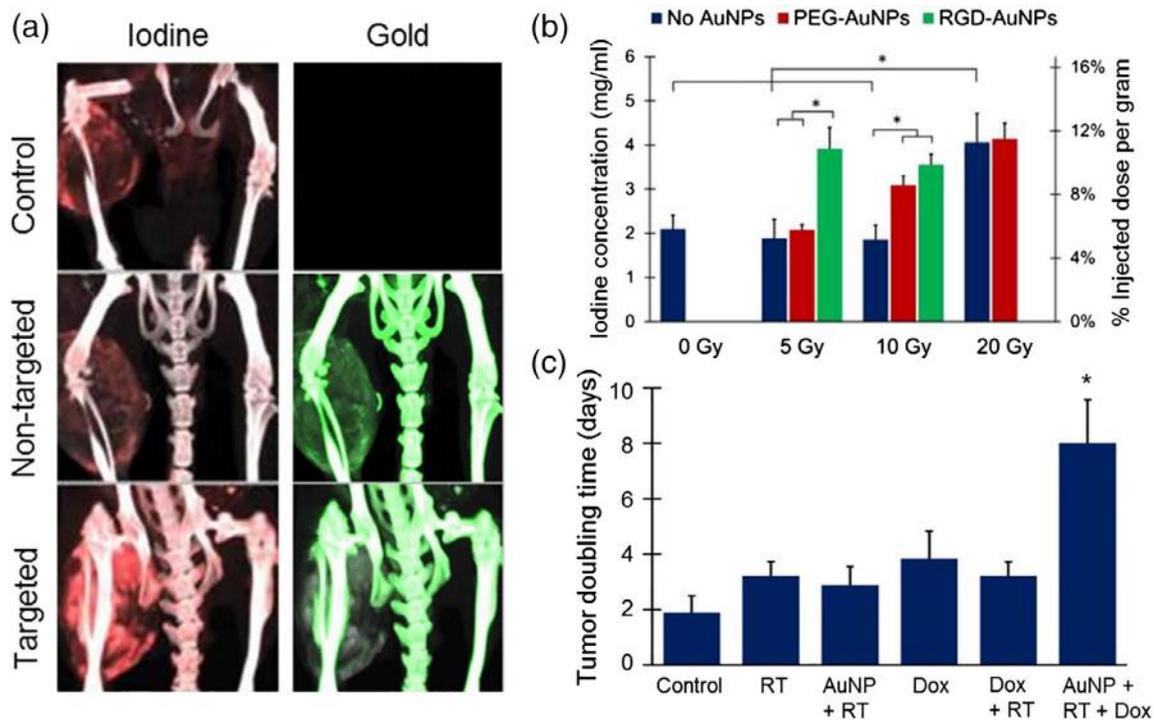
FIGURE 7 (a) DECT iodine and gold maps for hindlimb sarcomas in the groups treated with 5 Gy RT in conjunction with no AuNP (control), PEGylated AuNP (non-targeted), or RGD-functionalized AuNP (targeted). (b) Accumulation of liposomal iodine in the tumors following AuNP-augmented RT at varying radiation doses. (c) Tumor volume doubling time for mice treated with 5 Gy RT, targeted AuNP, and/or liposomal doxorubicin (Reprinted with permission from Ashton et al. (2018)). AuNP, gold nanoparticles; DECT, dual-energy CT; RT, radiotherapy

tissues with DEM, as mentioned above. Nevertheless, targeted agents should be further examined in additional animal models and their physicochemical properties should be optimized to elicit effective targeting.

3.2.5 | Cell tracking X-ray agents

Cell-based therapy is a promising direction for treating a variety of diseases, injuries, and disorders by transplanting living cells with therapeutic characteristics within the body (Greenfield & Hauser, 2018; McIntyre, Jones, Han, & Vangsness, 2018; Rosenberg & Restifo, 2015; Wu, Hu, & Wang, 2018). Understanding cell behavior in vivo offers fundamental knowledge on trafficking patterns and disease processes, and also allows evaluation of treatment effectiveness, which, taken together, can guide the development of cell-based therapies (Betzer, Meir, Motiei, Yadid, & Popovtzer, 2017; Bongso, Fong, & Gauthaman, 2008; Meir & Popovtzer, 2018). Current preclinical and clinical cell therapy experiments mainly employ three types of cells—stem cells, immune cells, and cancer cells (Cobos et al., 2014; Kang, Shin, Ko, Jo, & Ra, 2012; Park, Suryaprakash, Lao, & Leong, 2015; Rizk, Aziz, Shorr, & Allan, 2017). Another promising direction for cell-based therapies is the use of cell-derived exosomes as therapeutic agents and drug carriers (Chemla et al., 2019; Guo et al., 2019).

The development of accurate and sensitive noninvasive cell tracking techniques is a highly challenging task. Conservative methods for tracking cells, such as radionuclide-based or fluorescence-based techniques visualized by optical imaging, suffer from short half-lives or low tissue penetration, and therefore are not optimal for clinical use (Fixler, Garcia, Zalevsky, Weiss, & Deutsch, 2007; Srinivas et al., 2010). Nanoparticle-based contrast agents opened the door to a new era in cell tracking, with potential for application in humans (Meir & Popovtzer, 2018; Shilo, Reuveni, Motiei, & Popovtzer, 2012). The two core aspects for performing efficient cell tracking with nanoparticles are efficient cell labeling and in vivo imaging.

Cell tracking with X-ray CT is a rapidly developing field (J. Kim, Chhour, et al., 2017). Astolfo et al. (2013) provided the first evidence for in vivo cell tracking using AuNP combined with CT. Malignant cells were labeled with AuNP and

stereotactically injected to mouse brain. CT scans at 8 days postinjection revealed small clusters of cells (~1,700) in the brain. This work demonstrated the potential for monitoring the fate of injected cells while concomitantly studying the dynamics of a growing tumor by measuring its shape, volume, and division times, all via imaging.

Betzer et al. (2015) developed a protocol for labeling different types of cells with AuNP for in vivo applications (Figure 8a,b). This technology was applied in various mouse disease models for noninvasive CT monitoring of mesenchymal stem cell (MSC) in brain disorder treatment (Betzer et al., 2014; Shwartz et al., 2017), photoreceptor precursors in retinal replacement therapy (Chemla et al., 2019), and melanoma-specific T cells in cancer immunotherapy treatment (Figure 8c–f) (Meir et al., 2015). Design principles for cell tracking were further established using CT imaging after intramuscular stem cell transplantation in a mouse model of Duchenne muscular dystrophy. In these experiments, the minimum detection limit for cells was determined to be 500 cells, and a mathematical model was developed for quantifying the number of cells visualized in CT images (Meir et al., 2017). Interestingly, longitudinal cell tracking showed no signal loss up to 1 month after cell injection (Betzer et al., 2014).

To increase the detection sensitivity of CT, higher uptake of nanoparticles per cell is needed. T. Kim, Lee, et al. (2017) developed a straightforward method to label human MSCs with 40 nm AuNP complexed with poly-L-lysine (up to 600 pg per cell) and rhodamine B isothiocyanate to optimize in vivo visualization of therapeutic cells by micro-CT imaging. This approach allowed the quantification of cell numbers via CT, as the number of cells was linearly correlated with CT attenuation. It was determined that a minimum of 2×10^5 labeled human MSCs could be visualized with CT, which corresponded to a detection sensitivity threshold of $\approx 2 \times 10^4$ cells per μl.
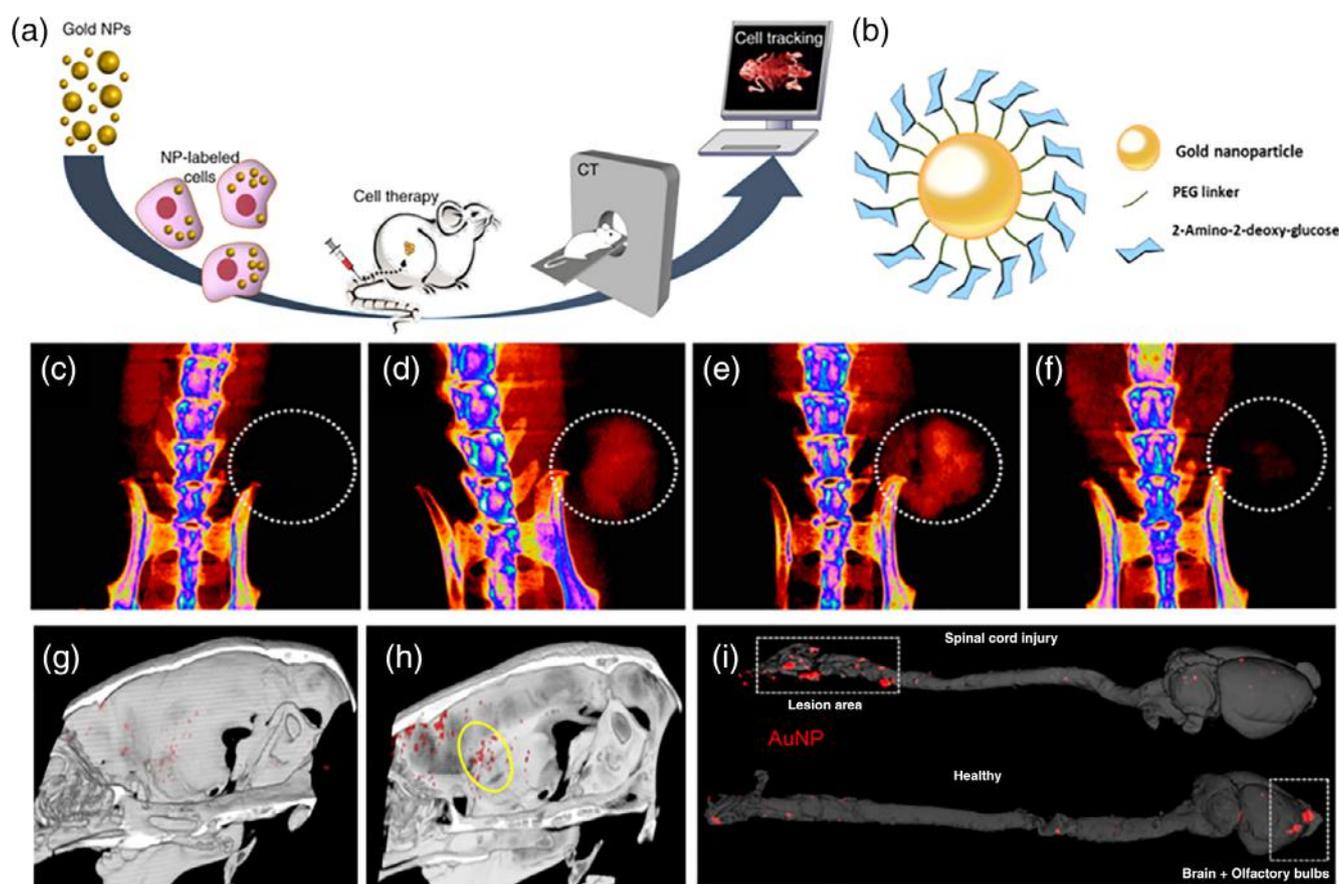

FIGURE 8 (a) Scheme showing the process of labeling cells with nanoparticles, followed by in vivo injection and CT imaging. (b) Schematic depiction of AuNP coated with glucose for labeling cells. In vivo CT imaging of the accumulation of antibody-targeted and AuNP-labeled T cells at a melanoma tumor in mouse: (c) before T-cell injection, (d) 24 hr post IV injection, (e) 48 hr postinjection, and (f) 72 hr postinjection. Circles demarcate the tumor area and the T-cell accumulation. In vivo CT imaging of gold-labeled exosomes in (g) control mouse brain, (h) striatal stroke region in a mouse model of acute stroke, and (i) a spinal cord lesion at 24 hr post intranasal administration of exosomes (Reprinted with permission from Betzer et al. (2015, 2017), Guo et al. (2019), and Meir et al. (2015)). AuNP, gold nanoparticles; CT, computed tomography

AuNP and CT are also effective for tracking immune cells in noncancerous diseases such as atherosclerosis. Chhour et al. (2017) performed a detailed study on the parameters that affect AuNP uptake by monocytes. Nanoparticles with numerous sizes and coatings were examined for optimal cell uptake. It was found that 15 nm AuNP coated with short carboxylic acid ligands as well as 50 and 75 nm AuNP coated with P-COOH were taken up extensively. These results show that cellular uptake of nanoparticles is strongly dependent on both size and surface functionality. Notably, the same group demonstrated the use of CT in tracking the migration of AuNP-labeled monocytes to atherosclerotic plaques and in observing the process of monocyte recruitment, which was shown to correlate with disease progression (Chhour et al., 2016).

Recently, several papers on in vivo CT tracking of exosomes have been published (Betzer et al., 2019; Betzer, Perets, et al., 2017; Guo et al., 2019; Perets et al., 2019). Exosomes, which are small vesicles shed by cells, act mainly as nanocarriers for cell-to-cell communication. Betzer, Perets, et al. (2017) developed a protocol for labeling MSC-derived exosomes with 5 nm glucose-coated AuNP and found intranasal injection to be the optimal administration route for neuroimaging of the exosomes. This tracking procedure was applied in several neurodegenerative and neurodevelopmental disorders, as it provides insight on the ability of these exosomes to cross the blood–brain-barrier, their migration patterns toward specific pathological regions, and the involvement of the immune system in the migration process (Figure 8g–i) (Perets et al., 2019).

Multimodal imaging is an excellent strategy for circumventing the inherent limitations of each imaging modality alone and enabling the examination of more than one process at a time. Arifin et al. (2011) developed multiplexed trimodal gadolinium-gold microcapsules that serve as contrast agents for CT, ultrasound, and MRI. Multimodal tracking of cells labeled with these microcapsules revealed that intra-abdominal cell transplantation restored normoglycemia in diabetic mice for up to 7 weeks. This multimodal imaging system enabled structural cell tracking together with the ability to track cell functionality.

In summary, recent studies have achieved significant advances in cell tracking using X-ray technologies. Further studies should be performed with a variety of nanoparticles and therapeutic cell types, in order to optimize cell labeling protocols and establish CT-guided cell tracking as a leading, reliable, and informative imaging concept.

4 | SUMMARY AND OUTLOOK

Overall, a burst of activity surrounding X-ray contrast agents having novel chemical compositions, allowing unique biomedical applications, and producing strong contrast for new X-ray imaging techniques has been seen in the past 15 years. An extensive array of compositions has been explored as X-ray contrast generating materials such as silver, gold, tantalum oxide, and bismuth sulfide. Most of these agents are nanoparticle-based and have potential as alternative X-ray contrast agents for patients for whom the use of current iodinated agents is contraindicated. Small, renally excretable gold, silver sulfide, or tantalum oxide nanoparticles have demonstrated great promise for future clinical translation. Improved blood pool agents with longer lasting contrast have been developed. Targeted and cell tracking agents have been reported for the detection of certain diseases and cell types, such as cancer and monocytes, via various X-ray imaging modalities. Advanced theranostic agents have also resulted in more effective disease planning and better treatment outcomes. In addition, candidate elements for novel contrast agent development for emerging X-ray imaging modalities, such as SPCCT, DEM, and photon-counting mammography, have recently been identified. With SPCCT, specific detection and quantification of contrast media as well as differentiation of tissue types are now possible.

An exciting new research area in the field involves the development of activatable agents that can provide differential image contrast as a response to environmental triggers such as pH or enzyme expression. For example, ROS degradable AuNP-polyphosphazene nanoprobes could be used to detect the presence of inflammation and cancer using bimodal PAI and CT imaging (Bouché et al., 2019). A switchable polymer-AuNP complex, which we have described above, could track the delivery of therapeutic drugs to diseased neurons via CT imaging (L. Liu et al., 2019). Furthermore, there has been a report of iodinated activity-based probes that produce detectable CT contrast based on activity-dependent covalent binding of cathepsin, an enzyme that is highly expressed in the tumor microenvironment (Gaikwad et al., 2018). Only a few examples of activatable X-ray contrast agents have been reported to date; however, this topic is gaining considerable interest and research around this agent type may bloom in the coming years.

Despite the positive outlook, further progress in synthetic approaches is required to develop these X-ray contrasting nanoparticles on a large scale and at low cost. Many emerging X-ray imaging modalities are still under development and their current system specifications and scanning conditions may vary from the final clinical scanner settings.

Hence, similar studies will need to be performed in refined systems and larger animal models to further validate the potential elements for development into novel contrast agents for X-ray imaging. More progress will be made in expanding the functions of current novel agents and also engineering nanoparticles with X-ray attenuating elements that are less explored, such as cerium, lanthanum, or molybdenum. While we were tasked with reviewing the field of nanoparticle X-ray contrast agents, advances are being made with other types of agent, such as metal chelates, which is also important work (Berger et al., 2017). It will be important for the field to focus research in the direction of clinical implementation. In order to achieve approval for use in patient care, thorough assessments on their long-term biodistribution, degradability, and toxicity will be needed to evaluate the issue of side effects and concerns related to their excretion profile. The field would advance further with greater interactions and more collaboration among chemists, medical physicists, radiologists, and clinicians to identify imaging needs and guide the development of novel contrast agents. Nevertheless, the field has seen tremendous advancement in the last few decades and we expect to see more exciting new discoveries in the near future.

ACKNOWLEDGMENTS

CONFLICT OF INTEREST

The authors have declared no conflicts of interest for this article.

AUTHOR CONTRIBUTIONS

Jessica Hsu: Conceptualization; investigation; writing-original draft; writing-review and editing. **Lenitza Nieves:** Investigation; writing-original draft; writing-review and editing. **Oshra Betzer:** Investigation; writing-original draft; writing-review and editing. **Tamar Sadan:** Investigation; writing-original draft; writing-review and editing. **Peter Noël:** Investigation; writing-original draft; writing-review and editing. **Rachela Popovtzer:** Investigation; resources; supervision; writing-review and editing. **David Cormode:** Conceptualization; investigation; resources; supervision; validation; writing-review and editing.

ORCID

Jessica C. Hsu https://orcid.org/0000-0002-3599-2834
Lenitza M. Nieves https://orcid.org/0000-0002-2241-1025
Rachela Popovtzer https://orcid.org/0000-0002-3585-348X
David P. Cormode https://orcid.org/0000-0002-8391-9500

RELATED WIREs ARTICLES

Cell tracking using gold nanoparticles and computed tomography imaging

REFERENCES

Al Zaki, A., Joh, D., Cheng, Z., De Barros, A. L., Kao, G., Dorsey, J., & Tsourkas, A. (2014). Gold-loaded polymeric micelles for computed tomography-guided radiation therapy treatment and radiosensitization. *ACS Nano*, *8*(1), 104–112.

Alvarez, R. E., & Macovski, A. (1976). Energy-selective reconstructions in X-ray computerized tomography. *Physics in Medicine and Biology*, *21*(5), 733–744.

Arifin, D. R., Long, C. M., Gilad, A. A., Alric, C., Roux, S., Tillement, O., ... Bulte, J. W. (2011). Trimodal gadolinium-gold microcapsules containing pancreatic islet cells restore normoglycemia in diabetic mice and can be tracked by using US, CT, and positive-contrast MR imaging. *Radiology*, *260*(3), 790–798.

Ashton, J. R., Castle, K. D., Qi, Y., Kirsch, D. G., West, J. L., & Badea, C. T. (2018). Dual-energy CT imaging of tumor liposome delivery after gold nanoparticle-augmented radiation therapy. *Theranostics*, *8*(7), 1782–1797.

Ashton, J. R., Clark, D. P., Moding, E. J., Ghaghada, K., Kirsch, D. G., West, J. L., & Badea, C. T. (2014). Dual-energy micro-CT functional imaging of primary lung cancer in mice using gold and iodine nanoparticle contrast agents: A validation study. *PLoS One*, *9*(2), e88129.

Astolfo, A., Schultke, E., Menk, R. H., Kirch, R. D., Juurlink, B. H., Hall, C., ... Arfelli, F. (2013). In vivo visualization of gold-loaded cells in mice using X-ray computed tomography. *Nanomedicine*, *9*(2), 284–292.

Behling, R. (2015). *Modern diagnostic X-ray sources: Technology, manufacturing, reliability*. Boca Raton, FL: CRC Press.

Berger, M., Bauser, M., Frenzel, T., Hilger, C. S., Jost, G., Lauria, S., ... Hegetschweiler, K. (2017). Hafnium-based contrast agents for X-ray computed tomography. *Inorganic Chemistry*, *56*(10), 5757–5761.

Betzer, O., Barnoy, E., Sadan, T., Elbaz, I., Braverman, C., Liu, Z., & Popovtzer, R. (2019). Advances in imaging strategies for in vivo tracking of exosomes. *Wiley Interdisciplinary Reviews: Nanomedicine and Nanobiotechnology*, 12, e1594.

Betzer, O., Meir, R., Dreifuss, T., Shamalov, K., Motiei, M., Shwartz, A., ... Popovtzer, R. (2015). In-vitro optimization of nanoparticle-cell labeling protocols for in-vivo cell tracking applications. *Scientific Reports*, 5, 15400.

Betzer, O., Meir, R., Motiei, M., Yadid, G., & Popovtzer, R. (2017). *Gold nanoparticle-cell labeling methodology for tracking stem cells within the brain* (Vol. 10077). Paper presented at the SPIE, San Francisco, California.

Betzer, O., Perets, N., Angel, A., Motiei, M., Sadan, T., Yadid, G., ... Popovtzer, R. (2017). In vivo neuroimaging of exosomes using gold nanoparticles. *ACS Nano*, 11(11), 10883–10893.

Betzer, O., Shilo, M., Opochinsky, R., Barnoy, E., Motiei, M., Okun, E., ... Popovtzer, R. (2017). The effect of nanoparticle size on the ability to cross the blood-brain barrier: An in vivo study. *Nanomedicine*, 12(13), 1533–1546.

Betzer, O., Shwartz, A., Motiei, M., Kazimirsky, G., Gispan, I., Damti, E., ... Popovtzer, R. (2014). Nanoparticle-based CT imaging technique for longitudinal and quantitative stem cell tracking within the brain: Application in neuropsychiatric disorders. *ACS Nano*, 8(9), 9274–9285.

Bongso, A., Fong, C. Y., & Gauthaman, K. (2008). Taking stem cells to the clinic: Major challenges. *Journal of Cellular Biochemistry*, 105(6), 1352–1360.

Bonitatibus, P. J., Jr., Torres, A. S., Goddard, G. D., FitzGerald, P. F., & Kulkarni, A. M. (2010). Synthesis, characterization, and computed tomography imaging of a tantalum oxide nanoparticle imaging agent. *Chemical Communications*, 46(47), 8956–8958.

Bonitatibus, P. J., Jr., Torres, A. S., Kandapallil, B., Lee, B. D., Goddard, G. D., Colborn, R. E., & Marino, M. E. (2012). Preclinical assessment of a zwitterionic tantalum oxide nanoparticle X-ray contrast agent. *ACS Nano*, 6(8), 6650–6658.

Bonvalot, S., Le Pechoux, C., De Baere, T., Kantor, G., Buy, X., Stoeckle, E., ... Soria, J. C. (2017). First-in-human study testing a new radioenhancer using nanoparticles (NBTXR3) activated by radiation therapy in patients with locally advanced soft tissue sarcomas. *Clinical Cancer Research*, 23(4), 908–917.

Bottinor, W., Polkampally, P., & Jovin, I. (2013). Adverse reactions to iodinated contrast media. *International Journal of Angiology*, 22(3), 149–154.

Bouché, M., Hsu, J. C., Dong, Y. C., Kim, J., Taing, K., & Cormode, D. P. (2020). Recent advances in molecular imaging with gold nanoparticles. *Bioconjugate Chemistry*, 31, 303–314.

Bouché, M., Puhringer, M., Iturmendi, A., Amirshaghaghi, A., Tsourkas, A., Teasdale, I., & Cormode, D. P. (2019). Activatable hybrid polyphosphazene-AuNP nanoprobe for ROS detection by bimodal PA/CT imaging. *ACS Applied Materials & Interfaces*, 11(32), 28648–28656.

Brown, A. L., & Goforth, A. M. (2012). pH-dependent synthesis and stability of aqueous, elemental bismuth glyconanoparticle colloids: Potentially biocompatible X-ray contrast agents. *Chemistry of Materials*, 24(9), 1599–1605.

Brown, A. L., Naha, P. C., Benavides-Montes, V., Litt, H. I., Goforth, A. M., & Cormode, D. P. (2014). Synthesis, X-ray opacity, and biological compatibility of ultra-high payload elemental bismuth nanoparticle X-ray contrast agents. *Chemistry of Materials*, 26(7), 2266–2274.

Cai, Q. Y., Kim, S. H., Choi, K. S., Kim, S. Y., Byun, S. J., Kim, K. W., ... Yoon, K. H. (2007). Colloidal gold nanoparticles as a blood-pool contrast agent for X-ray computed tomography in mice. *Investigative Radiology*, 42(12), 797–806.

Carrascosa, P., Capunay, C., Deviggiano, A., Bettinotti, M., Goldsmit, A., Tajer, C., ... Garcia, M. J. (2010). Feasibility of 64-slice gadolinium-enhanced cardiac CT for the evaluation of obstructive coronary artery disease. *Heart*, 96(19), 1543–1549.

Carton, A. K., Gavenonis, S. C., Currivan, J. A., Conant, E. F., Schnall, M. D., & Maidment, A. D. (2010). Dual-energy contrast-enhanced digital breast tomosynthesis—A feasibility study. *British Journal of Radiology*, 83(988), 344–350.

Carton, A. K., Ullberg, C., & Maidment, A. D. (2010). Optimization of a dual-energy contrast-enhanced technique for a photon-counting digital breast tomosynthesis system: II. An experimental validation. *Medical Physics*, 37(11), 5908–5913.

Chakravarty, S., Unold, J., Shuboni-Mulligan, D. D., Blanco-Fernandez, B., & Shapiro, E. M. (2016). Surface engineering of bismuth nanocrystals to counter dissolution. *Nanoscale*, 8(27), 13217–13222.

Cheheltani, R., Ezzibdeh, R. M., Chhour, P., Pulaparthi, K., Kim, J., Jurcova, M., ... Cormode, D. P. (2016). Tunable, biodegradable gold nanoparticles as contrast agents for computed tomography and photoacoustic imaging. *Biomaterials*, 102, 87–97.

Chemla, Y., Betzer, O., Markus, A., Farah, N., Motiei, M., Popovtzer, R., & Mandel, Y. (2019). Gold nanoparticles for multimodal high-resolution imaging of transplanted cells for retinal replacement therapy. *Nanomedicine*, 14(14), 1857–1871.

Chen, S. C., Carton, A. K., Albert, M., Conant, E. F., Schnall, M. D., & Maidment, A. D. (2007). Initial clinical experience with contrast-enhanced digital breast tomosynthesis. *Academic Radiology*, 14(2), 229–238.

Chen, X., Song, J., Chen, X., & Yang, H. (2019). X-ray-activated nanosystems for theranostic applications. *Chemical Society Reviews*, 48(11), 3073–3101.

Cheng, L., Liu, J., Gu, X., Gong, H., Shi, X., Liu, T., ... Liu, Z. (2014). PEGylated WS(2) nanosheets as a multifunctional theranostic agent for in vivo dual-modal CT/photoacoustic imaging guided photothermal therapy. *Advanced Materials*, 26(12), 1886–1893.

Chhour, P., Gallo, N., Cheheltani, R., Williams, D., Al-Zaki, A., Paik, T., ... Cormode, D. P. (2014). Nanodisco balls: Control over surface versus core loading of diagnostically active nanocrystals into polymer nanoparticles. *ACS Nano*, 8(9), 9143–9153.

Chhour, P., Kim, J., Benardo, B., Tovar, A., Mian, S., Litt, H. I., ... Cormode, D. P. (2017). Effect of gold nanoparticle size and coating on labeling monocytes for CT tracking. *Bioconjugate Chemistry*, 28(1), 260–269.

Chhour, P., Naha, P. C., O'Neill, S. M., Litt, H. I., Reilly, M. P., Ferrari, V. A., & Cormode, D. P. (2016). Labeling monocytes with gold nanoparticles to track their recruitment in atherosclerosis with computed tomography. *Biomaterials*, 87, 93–103.

Choi, H. S., Liu, W., Misra, P., Tanaka, E., Zimmer, J. P., Itty Ipe, B., ... Frangioni, J. V. (2007). Renal clearance of quantum dots. *Nature Biotechnology*, *25*(10), 1165–1170.

Chou, S. W., Shau, Y. H., Wu, P. C., Yang, Y. S., Shieh, D. B., & Chen, C. C. (2010). In vitro and in vivo studies of FePt nanoparticles for dual modal CT/MRI molecular imaging. *Journal of the American Chemical Society*, *132*(38), 13270–13278.

Clark, D. P., & Badea, C. T. (2014). Spectral diffusion: An algorithm for robust material decomposition of spectral CT data. *Physics in Medicine and Biology*, *59*(21), 6445–6466.

Cobos, C., Figueroa, J. A., Mirandola, L., Colombo, M., Summers, G., Figueroa, A., ... Cobos, E. (2014). The role of human papilloma virus (HPV) infection in non-anogenital cancer and the promise of immunotherapy: A review. *International Reviews of Immunology*, *33*(5), 383–401.

Cole, E. B., Toledano, A. Y., Lundqvist, M., & Pisano, E. D. (2012). Comparison of radiologist performance with photon-counting full-field digital mammography to conventional full-field digital mammography. *Academic Radiology*, *19*(8), 916–922.

Cole, L. E., McGinnity, T. L., Irimata, L. E., Vargo-Gogola, T., & Roeder, R. K. (2018). Effects of bisphosphonate ligands and PEGylation on targeted delivery of gold nanoparticles for contrast-enhanced radiographic detection of breast microcalcifications. *Acta Biomaterialia*, *82*, 122–132.

Cole, L. E., Ross, R. D., Tilley, J. M., Vargo-Gogola, T., & Roeder, R. K. (2015). Gold nanoparticles as contrast agents in X-ray imaging and computed tomography. *Nanomedicine*, *10*(2), 321–341.

Cole, L. E., Vargo-Gogola, T., & Roeder, R. K. (2014). Bisphosphonate-functionalized gold nanoparticles for contrast-enhanced X-ray detection of breast microcalcifications. *Biomaterials*, *35*(7), 2312–2321.

Cole, L. E., Vargo-Gogola, T., & Roeder, R. K. (2015). Contrast-enhanced X-ray detection of microcalcifications in radiographically dense mammary tissue using targeted gold nanoparticles. *ACS Nano*, *9*(9), 8923–8932.

Cormode, D. P., Naha, P. C., & Fayad, Z. A. (2014). Nanoparticle contrast agents for computed tomography: A focus on micelles. *Contrast Media & Molecular Imaging*, *9*(1), 37–52.

Cormode, D. P., Roessl, E., Thran, A., Skajaa, T., Gordon, R. E., Schlomka, J. P., ... Fayad, Z. A. (2010). Atherosclerotic plaque composition: Analysis with multicolor CT and targeted gold nanoparticles. *Radiology*, *256*(3), 774–782.

Cormode, D. P., Si-Mohamed, S., Bar-Ness, D., Sigovan, M., Naha, P. C., Balegamire, J., ... Douek, P. (2017). Multicolor spectral photon-counting computed tomography: in vivo dual contrast imaging with a high count rate scanner. *Scientific Reports*, *7*(1), 4784.

Cormode, D. P., Skajaa, T., van Schooneveld, M. M., Koole, R., Jarzyna, P., Lobatto, M. E., ... Mulder, W. J. (2008). Nanocrystal core high-density lipoproteins: A multimodality contrast agent platform. *Nano Letters*, *8*(11), 3715–3723.

Cui, Y., Yang, J., Zhou, Q., Liang, P., Wang, Y., Gao, X., & Wang, Y. (2017). Renal clearable Ag nanodots for in vivo computer tomography imaging and photothermal therapy. *ACS Applied Materials & Interfaces*, *9*(7), 5900–5906.

Curry, T., Kopelman, R., Shilo, M., & Popovtzer, R. (2014). Multifunctional theranostic gold nanoparticles for targeted CT imaging and photothermal therapy. *Contrast Media & Molecular Imaging*, *9*(1), 53–61.

De La Vega, J. C., & Hafeli, U. O. (2015). Utilization of nanoparticles as X-ray contrast agents for diagnostic imaging applications. *Contrast Media & Molecular Imaging*, *10*(2), 81–95.

Dean, P. B., Kivisaari, L., & Kormano, M. (1983). Contrast enhancement pharmacokinetics of six ionic and nonionic contrast media. *Investigative Radiology*, *18*(4), 368–374.

Diekmann, F., Freyer, M., Diekmann, S., Fallenberg, E. M., Fischer, T., Bick, U., & Pollinger, A. (2011). Evaluation of contrast-enhanced digital mammography. *European Journal of Radiology*, *78*(1), 112–121.

Ding, J., Wang, Y., Ma, M., Zhang, Y., Lu, S., Jiang, Y., ... Gu, N. (2013). CT/fluorescence dual-modal nanoemulsion platform for investigating atherosclerotic plaques. *Biomaterials*, *34*(1), 209–216.

Dong, L., Zhang, P., Liu, X., Deng, R., Du, K., Feng, J., & Zhang, H. (2019). Renal clearable Bi-Bi$_2$S$_3$ heterostructure nanoparticles for targeting cancer theranostics. *ACS Applied Materials & Interfaces*, *11*(8), 7774–7781.

Dong, Y. C., Hajfathalian, M., Maidment, P. S. N., Hsu, J. C., Naha, P. C., Si-Mohamed, S., ... Cormode, D. P. (2019). Effect of gold nanoparticle size on their properties as contrast agents for computed tomography. *Scientific Reports*, *9*(1), 14912.

Dou, Y., Guo, Y., Li, X., Li, X., Wang, S., Wang, L., ... Chang, J. (2016). Size-tuning ionization to optimize gold nanoparticles for simultaneous enhanced CT imaging and radiotherapy. *ACS Nano*, *10*(2), 2536–2548.

Dreifuss, T., Betzer, O., Shilo, M., Popovtzer, A., Motiei, M., & Popovtzer, R. (2015). A challenge for theranostics: Is the optimal particle for therapy also optimal for diagnostics? *Nanoscale*, *7*(37), 15175–15184.

Dromain, C., Thibault, F., Diekmann, F., Fallenberg, E. M., Jong, R. A., Koomen, M., ... Toledano, A. (2012). Dual-energy contrast-enhanced digital mammography: Initial clinical results of a multireader, multicase study. *Breast Cancer Research*, *14*(3), R94.

Du, B., Jiang, X., Das, A., Zhou, Q., Yu, M., Jin, R., & Zheng, J. (2017). Glomerular barrier behaves as an atomically precise bandpass filter in a sub-nanometre regime. *Nature Nanotechnology*, *12*(11), 1096–1102.

Du, B., Yu, M., & Zheng, J. (2018). Transport and interactions of nanoparticles in the kidneys. *Nature Reviews Materials*, *3*(10), 358–374.

Ehn, S., Sellerer, T., Mechlem, K., Fehringer, A., Epple, M., Herzen, J., ... Noël, P. B. (2017). Basis material decomposition in spectral CT using a semi-empirical, polychromatic adaption of the Beer-Lambert model. *Physics in Medicine and Biology*, *62*(1), N1–N17.

Ehn, S., Sellerer, T., Muenzel, D., Fingerle, A. A., Kopp, F., Duda, M., ... Noël, P. B. (2018). Assessment of quantification accuracy and image quality of a full-body dual-layer spectral CT system. *Journal of Applied Clinical Medical Physics*, *19*(1), 204–217.

Elrod, D. B., Partha, R., Danila, D., Casscells, S. W., & Conyers, J. L. (2009). An iodinated liposomal computed tomographic contrast agent prepared from a diiodophosphatidylcholine lipid. *Nanomedicine*, *5*(1), 42–45.

FitzGerald, P. F., Butts, M. D., Roberts, J. C., Colborn, R. E., Torres, A. S., Lee, B. D., ... Bonitatibus, P. J., Jr. (2016). A proposed computed tomography contrast agent using carboxybetaine zwitterionic tantalum oxide nanoparticles: Imaging, biological, and physicochemical performance. *Investigative Radiology*, 51(12), 786–796.

Fixler, D., Garcia, J., Zalevsky, Z., Weiss, A., & Deutsch, M. (2007). Speckle random coding for 2D super resolving fluorescent microscopic imaging. *Micron*, 38(2), 121–128.

Flohr, T. G., McCollough, C. H., Bruder, H., Petersilka, M., Gruber, K., Suss, C., ... Ohnesorge, B. M. (2006). First performance evaluation of a dual-source CT (DSCT) system. *European Radiology*, 16(2), 256–268.

Gaikwad, H. K., Tsvirkun, D., Ben-Nun, Y., Merquiol, E., Popovtzer, R., & Blum, G. (2018). Molecular imaging of cancer using X-ray computed tomography with protease targeted iodinated activity-based probes. *Nano Letters*, 18(3), 1582–1591.

Greenfield, A. L., & Hauser, S. L. (2018). B-cell therapy for multiple sclerosis: Entering an era. *Annals of Neurology*, 83(1), 13–26.

Gundogdu, O., Nirgianaki, E., Che Ismail, E., Jenneson, P. M., & Bradley, D. A. (2007). Benchtop phase-contrast X-ray imaging. *Applied Radiation and Isotopes*, 65(12), 1337–1344.

Guo, S., Perets, N., Betzer, O., Ben-Shaul, S., Sheinin, A., Michaelevski, I., ... Levenberg, S. (2019). Intranasal delivery of mesenchymal stem cell derived exosomes loaded with phosphatase and tensin homolog siRNA repairs complete spinal cord injury. *ACS Nano*, 13(9), 10015–10028.

Hainfeld, J. F., O'Connor, M. J., Dilmanian, F. A., Slatkin, D. N., Adams, D. J., & Smilowitz, H. M. (2011). Micro-CT enables microlocalisation and quantification of HER2-targeted gold nanoparticles within tumour regions. *British Journal of Radiology*, 84(1002), 526–533.

Hainfeld, J. F., Slatkin, D. N., Focella, T. M., & Smilowitz, H. M. (2006). Gold nanoparticles: A new X-ray contrast agent. *British Journal of Radiology*, 79(939), 248–253.

Hajfathalian, M., Amirshaghaghi, A., Naha, P. C., Chhour, P., Hsu, J. C., Douglas, K., ... Cormode, D. P. (2018). Wulff in a cage gold nanoparticles as contrast agents for computed tomography and photoacoustic imaging. *Nanoscale*, 10(39), 18749–18757.

Hallouard, F., Anton, N., Choquet, P., Constantinesco, A., & Vandamme, T. (2010). Iodinated blood pool contrast media for preclinical X-ray imaging applications—A review. *Biomaterials*, 31(24), 6249–6268.

Hallouard, F., Anton, N., Zuber, G., Choquet, P., Li, X., Arntz, Y., ... Vandamme, T. F. (2011). Radiopaque iodinated nano-emulsions for preclinical X-ray imaging. *RSC Advances*, 1(5), 792–801.

Hara, A. K., Paden, R. G., Silva, A. C., Kujak, J. L., Lawder, H. J., & Pavlicek, W. (2009). Iterative reconstruction technique for reducing body radiation dose at CT: Feasibility study. *American Journal of Roentgenology*, 193(3), 764–771.

Hazkani, I., Motiei, M., Betzer, O., Sadan, T., Bragilovski, D., Lubimov, L., ... Popovtzer, A. (2017). Can molecular profiling enhance radiotherapy? Impact of personalized targeted gold nanoparticles on radiosensitivity and imaging of adenoid cystic carcinoma. *Theranostics*, 7(16), 3962–3971.

Her, S., Jaffray, D. A., & Allen, C. (2017). Gold nanoparticles for applications in cancer radiotherapy: Mechanisms and recent advancements. *Advanced Drug Delivery Reviews*, 109, 84–101.

Hounsfield, G. N. (1973). Computerized transverse axial scanning (tomography). 1. Description of system. *British Journal of Radiology*, 46(552), 1016–1022.

Hsu, J. C., Cruz, E. D., Lau, K. C., Bouché, M., Kim, J., Maidment, A. D. A., & Cormode, D. P. (2019). Renally excretable and size-tunable silver sulfide nanoparticles for dual-energy mammography or computed tomography. *Chemistry of Materials*, 31(19), 7845–7854.

Hsu, J. C., Naha, P. C., Lau, K. C., Chhour, P., Hastings, R., Moon, B. F., ... Cormode, D. P. (2018). An all-in-one nanoparticle (AION) contrast agent for breast cancer screening with DEM-CT-MRI-NIRF imaging. *Nanoscale*, 10(36), 17236–17248.

Hu, X., Sun, J., Li, F., Li, R., Wu, J., He, J., ... Ling, D. (2018). Renal-clearable hollow bismuth subcarbonate nanotubes for tumor targeted computed tomography imaging and chemoradiotherapy. *Nano Letters*, 18(2), 1196–1204.

Huang, P., Bao, L., Zhang, C., Lin, J., Luo, T., Yang, D., ... Cui, D. (2011). Folic acid-conjugated silica-modified gold nanorods for X-ray/CT imaging-guided dual-mode radiation and photo-thermal therapy. *Biomaterials*, 32(36), 9796–9809.

Huo, S., Chen, S., Gong, N., Liu, J., Li, X., Zhao, Y., & Liang, X. J. (2017). Ultrasmall gold nanoparticles behavior in vivo modulated by surface polyethylene glycol (PEG) grafting. *Bioconjugate Chemistry*, 28(1), 239–243.

Hussain, Z., Khan, S., Imran, M., Sohail, M., Shah, S. W. A., & de Matas, M. (2019). PEGylation: A promising strategy to overcome challenges to cancer-targeted nanomedicines: A review of challenges to clinical transition and promising resolution. *Drug Delivery and Translational Research*, 9(3), 721–734.

Hyafil, F., Cornily, J. C., Feig, J. E., Gordon, R., Vucic, E., Amirbekian, V., ... Fayad, Z. A. (2007). Noninvasive detection of macrophages using a nanoparticulate contrast agent for computed tomography. *Nature Medicine*, 13(5), 636–641.

Jackson, P., Periasamy, S., Bansal, V., & Geso, M. (2011). Evaluation of the effects of gold nanoparticle shape and size on contrast enhancement in radiological imaging. *Australasian Physical & Engineering Sciences in Medicine*, 34(2), 243–249.

Jarzyna, P. A., Gianella, A., Skajaa, T., Knudsen, G., Deddens, L. H., Cormode, D. P., ... Mulder, W. J. (2010). Multifunctional imaging nanoprobes. *Wiley Interdisciplinary Reviews: Nanomedicine and Nanobiotechnology*, 2(2), 138–150.

Jin, Y., Ma, X., Feng, S., Liang, X., Dai, Z., Tian, J., & Yue, X. (2015). Hyaluronic acid modified tantalum oxide nanoparticles conjugating doxorubicin for targeted cancer theranostics. *Bioconjugate Chemistry*, 26(12), 2530–2541.

Jin, Y., Ma, X., Zhang, S., Meng, H., Xu, M., Yang, X., ... Tian, J. (2017). A tantalum oxide-based core/shell nanoparticle for triple-modality image-guided chemo-thermal synergetic therapy of esophageal carcinoma. *Cancer Letters*, 397, 61–71.

Jing, L., Liang, X., Deng, Z., Feng, S., Li, X., Huang, M., ... Dai, Z. (2014). Prussian blue coated gold nanoparticles for simultaneous photoacoustic/CT bimodal imaging and photothermal ablation of cancer. *Biomaterials*, 35(22), 5814–5821.

Johnson, T. R., Nikolaou, K., Wintersperger, B. J., Leber, A. W., von Ziegler, F., Rist, C., ... Becker, C. R. (2006). Dual-source CT cardiac imaging: Initial experience. *European Radiology*, *16*(7), 1409–1415.

Kang, S. K., Shin, I. S., Ko, M. S., Jo, J. Y., & Ra, J. C. (2012). Journey of mesenchymal stem cells for homing: Strategies to enhance efficacy and safety of stem cell therapy. *Stem Cells International*, *2012*, 342968.

Karunamuni, R., & Maidment, A. D. (2014). Search for novel contrast materials in dual-energy X-ray breast imaging using theoretical modeling of contrast-to-noise ratio. *Physics in Medicine and Biology*, *59*(15), 4311–4324.

Karunamuni, R., Naha, P. C., Lau, K. C., Al-Zaki, A., Popov, A. V., Delikatny, E. J., ... Maidment, A. D. (2016). Development of silica-encapsulated silver nanoparticles as contrast agents intended for dual-energy mammography. *European Radiology*, *26*(9), 3301–3309.

Karunamuni, R., Tsourkas, A., & Maidment, A. D. (2014). Exploring silver as a contrast agent for contrast-enhanced dual-energy X-ray breast imaging. *British Journal of Radiology*, *87*(1041), 20140081.

Khademi, S., Sarkar, S., Shakeri-Zadeh, A., Attaran, N., Kharrazi, S., Ay, M. R., & Ghadiri, H. (2018). Folic acid-cysteamine modified gold nanoparticle as a nanoprobe for targeted computed tomography imaging of cancer cells. *Materials Science & Engineering C: Materials for Biological Applications*, *89*, 182–193.

Kim, J., Bar-Ness, D., Si-Mohamed, S., Coulon, P., Blevis, I., Douek, P., & Cormode, D. P. (2018). Assessment of candidate elements for development of spectral photon-counting CT specific contrast agents. *Scientific Reports*, *8*(1), 12119.

Kim, J., Chhour, P., Hsu, J., Litt, H. I., Ferrari, V. A., Popovtzer, R., & Cormode, D. P. (2017). Use of nanoparticle contrast agents for cell tracking with computed tomography. *Bioconjugate Chemistry*, *28*(6), 1581–1597.

Kim, J., Silva, A. B., Hsu, J. C., Maidment, P. S. N., Shapira, N., Noël, P. B., & Cormode, D. P. (2019). Radioprotective garment-inspired biodegradable polymetal nanoparticles for enhanced CT contrast production. *Chemistry of Materials*, *32*(1), 381–391.

Kim, J. Y., Ryu, J. H., Schellingerhout, D., Sun, I. C., Lee, S. K., Jeon, S., ... Kim, D. E. (2015). Direct imaging of cerebral thromboemboli using computed tomography and fibrin-targeted gold nanoparticles. *Theranostics*, *5*(10), 1098–1114.

Kim, T., Lee, N., Arifin, D. R., Shats, I., Janowski, M., Walczak, P., ... Bulte, J. W. M. (2017). In vivo micro-CT imaging of human mesenchymal stem cells labeled with gold-poly-l-lysine nanocomplexes. *Advanced Functional Materials*, *27*(3), 1604213.

Kodiyan, A., Silva, E. A., Kim, J., Aizenberg, M., & Mooney, D. J. (2012). Surface modification with alginate-derived polymers for stable, protein-repellent, long-circulating gold nanoparticles. *ACS Nano*, *6*(6), 4796–4805.

Krauss, B., & McCollough, C. H. (2019). Dual energy and spectral CT techniques in cardiovascular imaging. In *CT of the heart* (pp. 87–101). Totowa, NJ: Humana.

Kwon, S. P., Jeon, S., Lee, S. H., Yoon, H. Y., Ryu, J. H., Choi, D., ... Ahn, C. H. (2018). Thrombin-activatable fluorescent peptide incorporated gold nanoparticles for dual optical/computed tomography thrombus imaging. *Biomaterials*, *150*, 125–136.

Laakkonen, P., Porkka, K., Hoffman, J. A., & Ruoslahti, E. (2002). A tumor-homing peptide with a targeting specificity related to lymphatic vessels. *Nature Medicine*, *8*(7), 751–755.

Lau, K., Hsu, J., Cederström, B., Cormode, D., & Maidment, A. (2019). *Evaluation of silver sulfide nanoparticles as a contrast agent for spectral photon-counting digital mammography: A phantom study* (Vol. 10948). Paper presented at the SPIE, San Diego, California.

Lau, K., Hsu, J., Naha, P., Chhour, P., Hastings, R., Stein, J., ... Maidment, A. D. (2018). *Acquisition parameters for dual-energy contrast-enhanced digital mammography using a micelle-based all-in-one nanoparticle (AION) contrast agent: A phantom study* (Vol. 10718). Paper presented at the SPIE, Atlanta, Georgia.

Lee, N., Choi, S. H., & Hyeon, T. (2013). Nano-sized CT contrast agents. *Advanced Materials*, *25*(19), 2641–2660.

Lei, P., An, R., Zhang, P., Yao, S., Song, S., Dong, L., ... Zhang, H. (2017). Ultrafast synthesis of ultrasmall poly(vinylpyrrolidone)-protected bismuth nanodots as a multifunctional theranostic agent for in vivo dual-modal CT/photothermal-imaging-guided photothermal therapy. *Advanced Functional Materials*, *27*(35), 1702018.

Levine, D., McDonald, R. J., & Kressel, H. Y. (2018). Gadolinium retention after contrast-enhanced MRI. *The Journal of the American Medical Association*, *320*(18), 1853–1854.

Lewin, J. M. (2008). Digital mammography. In *Cancer imaging*. Boston, MA: Elsevier Academic Press.

Li, J., Hu, Y., Yang, J., Wei, P., Sun, W., Shen, M., ... Shi, X. (2015). Hyaluronic acid-modified Fe_3O_4@Au core/shell nanostars for multimodal imaging and photothermal therapy of tumors. *Biomaterials*, *38*, 10–21.

Li, L., Lu, Y., Jiang, C., Zhu, Y., Yang, X., Hu, X., ... Mao, C. (2018). Actively targeted deep tissue imaging and photothermal-chemo therapy of breast cancer by antibody-functionalized drug-loaded X-ray-responsive bismuth sulfide@mesoporous silica core-shell nanoparticles. *Advanced Functional Materials*, *28*(5), 1704623.

Li, X., Anton, N., Zuber, G., & Vandamme, T. (2014). Contrast agents for preclinical targeted X-ray imaging. *Advanced Drug Delivery Reviews*, *76*, 116–133.

Li, Z., Hu, Y., Miao, Z., Xu, H., Li, C., Zhao, Y., ... Yu, M. (2018). Dual-stimuli responsive bismuth nanoraspberries for multimodal imaging and combined cancer therapy. *Nano Letters*, *18*(11), 6778–6788.

Li, Z., Liu, J., Hu, Y., Li, Z., Fan, X., Sun, Y., ... Yu, M. (2017). Biocompatible PEGylated bismuth nanocrystals: "All-in-one" theranostic agent with triple-modal imaging and efficient in vivo photothermal ablation of tumors. *Biomaterials*, *141*, 284–295.

Lin, J., Hu, W., Gao, F., Qin, J., Peng, C., & Lu, X. (2018). Folic acid-modified diatrizoic acid-linked dendrimer-entrapped gold nanoparticles enable targeted CT imaging of human cervical cancer. *Journal of Cancer*, *9*(3), 564–577.

Lin, W., Zhang, X., Qian, L., Yao, N., Pan, Y., & Zhang, L. (2017). Doxorubicin-loaded unimolecular micelle-stabilized gold nanoparticles as a theranostic nanoplatform for tumor-targeted chemotherapy and computed tomography imaging. *Biomacromolecules*, *18*(12), 3869–3880.

Liu, J., Yu, M., Zhou, C., & Zheng, J. (2013). Renal clearable inorganic nanoparticles: A new frontier of bionanotechnology. *Materials Today*, *16*(12), 477–486.

Liu, J., Zheng, X., Yan, L., Zhou, L., Tian, G., Yin, W., ... Zhao, Y. (2015). Bismuth sulfide nanorods as a precision nanomedicine for in vivo multimodal imaging-guided photothermal therapy of tumor. *ACS Nano*, *9*(1), 696–707.

Liu, L., Li, Y., Liu, R., Shen, Q., Li, Y., Shi, Z., ... Zhang, X. (2019). Switchable nanoparticle for programmed gene-chem delivery with enhanced neuronal recovery and CT imaging for neurodegenerative disease treatment. *Materials Horizons*, *6*(9), 1923–1929.

Liu, M., Anderson, R. C., Lan, X., Conti, P. S., & Chen, K. (2020). Recent advances in the development of nanoparticles for multimodality imaging and therapy of cancer. *Medicinal Research Reviews*, *40*, 909–930.

Lohofer, F. K., Kaissis, G. A., Koster, F. L., Ziegelmayer, S., Einspieler, I., Gerngross, C., ... Braren, R. F. (2018). Improved detection rates and treatment planning of head and neck cancer using dual-layer spectral CT. *European Radiology*, *28*(12), 4925–4931.

Lu, Y., Li, L., Lin, Z., Li, M., Hu, X., Zhang, Y., ... Han, G. (2018). Enhancing osteosarcoma killing and CT imaging using ultrahigh drug loading and NIR-responsive bismuth sulfide@mesoporous silica nanoparticles. *Advanced Healthcare Materials*, *7*(19), e1800602.

Maass, C., Baer, M., & Kachelriess, M. (2009). Image-based dual energy CT using optimized precorrection functions: A practical new approach of material decomposition in image domain. *Medical Physics*, *36*(8), 3818–3829.

Maguire, C. M., Rosslein, M., Wick, P., & Prina-Mello, A. (2018). Characterisation of particles in solution—A perspective on light scattering and comparative technologies. *Science and Technology of Advanced Materials*, *19*(1), 732–745.

Mao, F., Wen, L., Sun, C., Zhang, S., Wang, G., Zeng, J., ... Li, Z. (2016). Ultrasmall biocompatible Bi_2Se_3 nanodots for multimodal imaging-guided synergistic radiophotothermal therapy against cancer. *ACS Nano*, *10*(12), 11145–11155.

McCollough, C. H., Leng, S., Yu, L., & Fletcher, J. G. (2015). Dual- and multi-energy CT: Principles, technical approaches, and clinical applications. *Radiology*, *276*(3), 637–653.

McDonald, R. J., McDonald, J. S., Kallmes, D. F., Jentoft, M. E., Murray, D. L., Thielen, K. R., ... Eckel, L. J. (2015). Intracranial gadolinium deposition after contrast-enhanced MR imaging. *Radiology*, *275*(3), 772–782.

McIntyre, J. A., Jones, I. A., Han, B., & Vangsness, C. T., Jr. (2018). Intra-articular mesenchymal stem cell therapy for the human joint: A systematic review. *American Journal of Sports Medicine*, *46*(14), 3550–3563.

McQuade, C., Al Zaki, A., Desai, Y., Vido, M., Sakhuja, T., Cheng, Z., ... Tsourkas, A. (2015). A multifunctional nanoplatform for imaging, radiotherapy, and the prediction of therapeutic response. *Small*, *11*(7), 834–843.

Meir, R., Betzer, O., Motiei, M., Kronfeld, N., Brodie, C., & Popovtzer, R. (2017). Design principles for noninvasive, longitudinal and quantitative cell tracking with nanoparticle-based CT imaging. *Nanomedicine*, *13*(2), 421–429.

Meir, R., & Popovtzer, R. (2018). Cell tracking using gold nanoparticles and computed tomography imaging. *Wiley Interdisciplinary Reviews: Nanomedicine and Nanobiotechnology*, *10*(2), e1480.

Meir, R., Shamalov, K., Betzer, O., Motiei, M., Horovitz-Fried, M., Yehuda, R., ... Cohen, C. J. (2015). Nanomedicine for cancer immunotherapy: Tracking cancer-specific T-cells in vivo with gold nanoparticles and CT imaging. *ACS Nano*, *9*(6), 6363–6372.

Meir, R., Shamalov, K., Sadan, T., Motiei, M., Yaari, G., Cohen, C. J., & Popovtzer, R. (2017). Fast image-guided stratification using anti-programmed death ligand 1 gold nanoparticles for cancer immunotherapy. *ACS Nano*, *11*(11), 11127–11134.

Menon, M. C., Chuang, P. Y., & He, C. J. (2012). The glomerular filtration barrier: Components and crosstalk. *International Journal of Nephrology*, *2012*, 749010.

Muenzel, D., Bar-Ness, D., Roessl, E., Blevis, I., Bartels, M., Fingerle, A. A., ... Noël, P. B. (2017). Spectral photon-counting CT: Initial experience with dual-contrast agent k-edge colonography. *Radiology*, *283*(3), 723–728.

Mukundan, S., Jr., Ghaghada, K. B., Badea, C. T., Kao, C. Y., Hedlund, L. W., Provenzale, J. M., ... Annapragada, A. (2006). A liposomal nanoscale contrast agent for preclinical CT in mice. *American Journal of Roentgenology*, *186*(2), 300–307.

Naha, P. C., Lau, K. C., Hsu, J. C., Hajfathalian, M., Mian, S., Chhour, P., ... Cormode, D. P. (2016). Gold silver alloy nanoparticles (GSAN): An imaging probe for breast cancer screening with dual-energy mammography or computed tomography. *Nanoscale*, *8*(28), 13740–13754.

Naha, P. C., Zaki, A. A., Hecht, E., Chorny, M., Chhour, P., Blankemeyer, E., ... Cormode, D. P. (2014). Dextran coated bismuth-iron oxide nanohybrid contrast agents for computed tomography and magnetic resonance imaging. *Journal of Materials Chemistry B*, *2*(46), 8239–8248.

Noël, P. B., Renger, B., Fiebich, M., Munzel, D., Fingerle, A. A., Rummeny, E. J., & Dobritz, M. (2013). Does iterative reconstruction lower CT radiation dose: Evaluation of 15,000 examinations. *PLoS One*, *8*(11), e81141.

Nowak, T., Hupfer, M., Brauweiler, R., Eisa, F., & Kalender, W. A. (2011). Potential of high-Z contrast agents in clinical contrast-enhanced computed tomography. *Medical Physics*, *38*(12), 6469–6482.

O'Donnell, T., Halaweish, A., Cormode, D. P., Cheheltani, R., Fayad, Z. A., & Mani, V. (2017). Material decomposition in an arbitrary number of dimensions using noise compensating projection. *Biomedical Physics & Engineering Express*, *4*(1), 015007.

OECD. (2020). Computed tomography (CT) exams (indicator). Retrieved from https://doi.org/10.1787/3c994537-en.

Oliva, M. R., Erturk, S. M., Ichikawa, T., Rocha, T., Ros, P. R., Silverman, S. G., & Mortele, K. J. (2012). Gastrointestinal tract wall visualization and distention during abdominal and pelvic multidetector CT with a neutral barium sulphate suspension: Comparison with positive barium sulphate suspension and with water. *JBR-BTR*, *95*(4), 237–242.

Pan, D., Roessl, E., Schlomka, J. P., Caruthers, S. D., Senpan, A., Scott, M. J., ... Lanza, G. M. (2010). Computed tomography in color: NanoK-enhanced spectral CT molecular imaging. *Angewandte Chemie International Edition English*, *49*(50), 9635–9639.

Pan, D., Schirra, C. O., Senpan, A., Schmieder, A. H., Stacy, A. J., Roessl, E., ... Lanza, G. M. (2012). An early investigation of ytterbium nanocolloids for selective and quantitative "multicolor" spectral CT imaging. *ACS Nano*, *6*(4), 3364–3370.

Pan, D., Williams, T. A., Senpan, A., Allen, J. S., Scott, M. J., Gaffney, P. J., ... Lanza, G. M. (2009). Detecting vascular biosignatures with a colloidal, radio-opaque polymeric nanoparticle. *Journal of the American Chemical Society*, *131*(42), 15522–15527.

Park, J. S., Suryaprakash, S., Lao, Y. H., & Leong, K. W. (2015). Engineering mesenchymal stem cells for regenerative medicine and drug delivery. *Methods*, *84*, 3–16.

Pelgrim, G. J., van Hamersvelt, R. W., Willemink, M. J., Schmidt, B. T., Flohr, T., Schilham, A., ... Vliegenthart, R. (2017). Accuracy of iodine quantification using dual energy CT in latest generation dual source and dual layer CT. *European Radiology*, *27*(9), 3904–3912.

Perets, N., Betzer, O., Shapira, R., Brenstein, S., Angel, A., Sadan, T., ... Offen, D. (2019). Golden exosomes selectively target brain pathologies in neurodegenerative and neurodevelopmental disorders. *Nano Letters*, *19*(6), 3422–3431.

Piao, J. G., Wang, L. M., Gao, F., You, Y. Z., Xiong, Y. J., & Yang, L. H. (2014). Erythrocyte membrane is an alternative coating to polyethylene glycol for prolonging the circulation lifetime of gold nanocages for photothermal therapy. *ACS Nano*, *8*(10), 10414–10425.

Pinho, D. F., Kulkarni, N. M., Krishnaraj, A., Kalva, S. P., & Sahani, D. V. (2013). Initial experience with single-source dual-energy CT abdominal angiography and comparison with single-energy CT angiography: Image quality, enhancement, diagnosis and radiation dose. *European Radiology*, *23*(2), 351–359.

Postma, A. A., Das, M., Stadler, A. A., & Wildberger, J. E. (2015). Dual-energy CT: What the neuroradiologist should know. *Current Radiology Reports*, *3*(5), 16.

Pourmorteza, A., Symons, R., Sandfort, V., Mallek, M., Fuld, M. K., Henderson, G., ... Bluemke, D. A. (2016). Abdominal imaging with contrast-enhanced photon-counting CT: First human experience. *Radiology*, *279*(1), 239–245.

Prakash, P., Kalra, M. K., Kambadakone, A. K., Pien, H., Hsieh, J., Blake, M. A., & Sahani, D. V. (2010). Reducing abdominal CT radiation dose with adaptive statistical iterative reconstruction technique. *Investigative Radiology*, *45*(4), 202–210.

Rabin, O., Manuel Perez, J., Grimm, J., Wojtkiewicz, G., & Weissleder, R. (2006). An X-ray computed tomography imaging agent based on long-circulating bismuth sulphide nanoparticles. *Nature Materials*, *5*(2), 118–122.

Reuveni, T., Motiei, M., Romman, Z., Popovtzer, A., & Popovtzer, R. (2011). Targeted gold nanoparticles enable molecular CT imaging of cancer: An in vivo study. *International Journal of Nanomedicine*, *6*, 2859–2864.

Rizk, M., Aziz, J., Shorr, R., & Allan, D. S. (2017). Cell-based therapy using umbilical cord blood for novel indications in regenerative therapy and immune modulation: An updated systematic scoping review of the literature. *Biology of Blood and Marrow Transplantation*, *23*(10), 1607–1613.

Roessl, E., & Proksa, R. (2007). K-edge imaging in X-ray computed tomography using multi-bin photon counting detectors. *Physics in Medicine and Biology*, *52*(15), 4679–4696.

Roessler, A. C., Hupfer, M., Kolditz, D., Jost, G., Pietsch, H., & Kalender, W. A. (2016). High atomic number contrast media offer potential for radiation dose reduction in contrast-enhanced computed tomography. *Investigative Radiology*, *51*(4), 249–254.

Rosenberg, S. A., & Restifo, N. P. (2015). Adoptive cell transfer as personalized immunotherapy for human cancer. *Science*, *348*(6230), 62–68.

Ross, R. D., Cole, L. E., Tilley, J. M. R., & Roeder, R. K. (2014). Effects of functionalized gold nanoparticle size on X-ray attenuation and substrate binding affinity. *Chemistry of Materials*, *26*(2), 1187–1194.

Russo, P. (2018). *Handbook of X-ray imaging: Physics and technology*. Boca Raton, FL: CRC Press.

Sauter, A. P., Kopp, F. K., Munzel, D., Dangelmaier, J., Renz, M., Renger, B., ... Noël, P. B. (2018). Accuracy of iodine quantification in dual-layer spectral CT: Influence of iterative reconstruction, patient habitus and tube parameters. *European Journal of Radiology*, *102*, 83–88.

Schirra, C. O., Senpan, A., Roessl, E., Thran, A., Stacy, A. J., Wu, L., ... Pan, D. (2012). Second generation gold nanobeacons for robust k-edge imaging with multi-energy CT. *Journal of Materials Chemistry*, *22*(43), 23071–23077.

Schlomka, J. P., Roessl, E., Dorscheid, R., Dill, S., Martens, G., Istel, T., ... Proksa, R. (2008). Experimental feasibility of multi-energy photon-counting K-edge imaging in pre-clinical computed tomography. *Physics in Medicine and Biology*, *53*(15), 4031–4047.

Schmid-Bindert, G., Henzler, T., Chu, T. Q., Meyer, M., Nance, J. W., Jr., Schoepf, U. J., ... Fink, C. (2012). Functional imaging of lung cancer using dual energy CT: How does iodine related attenuation correlate with standardized uptake value of 18FDG-PET-CT? *European Radiology*, *22*(1), 93–103.

Schmitz, S. A., Wagner, S., Schuhmann-Giampieri, G., Krause, W., & Wolf, K. J. (1997). A prototype liver-specific contrast medium for CT: Preclinical evaluation of gadoxetic acid disodium, or Gd-EOB-DTPA. *Radiology*, *202*(2), 407–412.

Scott, R. P., & Quaggin, S. E. (2015). Review series: The cell biology of renal filtration. *Journal of Cell Biology*, *209*(2), 199–210.

Selinger, M., & Koff, R. S. (1975). Thorotrast and the liver: A reminder. *Gastroenterology*, *68*(4), 799–803.

Shilo, M., Motiei, M., Hana, P., & Popovtzer, R. (2014). Transport of nanoparticles through the blood-brain barrier for imaging and therapeutic applications. *Nanoscale*, *6*(4), 2146–2152.

Shilo, M., Reuveni, T., Motiei, M., & Popovtzer, R. (2012). Nanoparticles as computed tomography contrast agents: Current status and future perspectives. *Nanomedicine*, *7*(2), 257–269.

Shwartz, A., Betzer, O., Kronfeld, N., Kazimirsky, G., Cazacu, S., Finniss, S., ... Yadid, G. (2017). Therapeutic effect of astroglia-like mesenchymal stem cells expressing glutamate transporter in a genetic rat model of depression. *Theranostics*, *7*(10), 2690–2703.

Si-Mohamed, S., Bar-Ness, D., Sigovan, M., Cormode, D. P., Coulon, P., Coche, E., … Douek, P. (2017). Review of an initial experience with an experimental spectral photon-counting computed tomography system. *Nuclear Instruments and Methods in Physics Research Section A: Accelerators, Spectrometers, Detectors and Associated Equipment*, *873*, 27–35.

Si-Mohamed, S., Bar-Ness, D., Sigovan, M., Tatard-Leitman, V., Cormode, D. P., Naha, P. C., … Douek, P. (2018). Multicolour imaging with spectral photon-counting CT: A phantom study. *European Radiology Experimental*, *2*(1), 34.

Si-Mohamed, S., Cormode, D. P., Bar-Ness, D., Sigovan, M., Naha, P. C., Langlois, J. B., … Douek, P. (2017). Evaluation of spectral photon counting computed tomography k-edge imaging for determination of gold nanoparticle biodistribution in vivo. *Nanoscale*, *9*(46), 18246–18257.

Si-Mohamed, S., Thivolet, A., Bonnot, P. E., Bar-Ness, D., Kepenekian, V., Cormode, D. P., … Rousset, P. (2018). Improved peritoneal cavity and abdominal organ imaging using a biphasic contrast agent protocol and spectral photon counting computed tomography k-edge imaging. *Investigative Radiology*, *53*(10), 629–639.

Skaane, P., Bandos, A. I., Gullien, R., Eben, E. B., Ekseth, U., Haakenaasen, U., … Gur, D. (2013). Comparison of digital mammography alone and digital mammography plus tomosynthesis in a population-based screening program. *Radiology*, *267*(1), 47–56.

Srinivas, M., Aarntzen, E. H., Bulte, J. W., Oyen, W. J., Heerschap, A., de Vries, I. J., & Figdor, C. G. (2010). Imaging of cellular therapies. *Advanced Drug Delivery Reviews*, *62*(11), 1080–1093.

Suk, J. S., Xu, Q. G., Kim, N., Hanes, J., & Ensign, L. M. (2016). PEGylation as a strategy for improving nanoparticle-based drug and gene delivery. *Advanced Drug Delivery Reviews*, *99*, 28–51.

Sykes, E. A., Chen, J., Zheng, G., & Chan, W. C. (2014). Investigating the impact of nanoparticle size on active and passive tumor targeting efficiency. *ACS Nano*, *8*(6), 5696–5706.

Taguchi, K. (2017). Energy-sensitive photon counting detector-based X-ray computed tomography. *Radiological Physics and Technology*, *10*(1), 8–22.

Tang, D., Gao, W., Yuan, Y., Guo, L., & Mei, X. (2017). Novel biocompatible Au nanostars@PEG nanoparticles for in vivo CT imaging and renal clearance properties. *Nanoscale Research Letters*, *12*(1), 565.

Tang, S., Peng, C., Xu, J., Du, B., Wang, Q., Vinluan, R. D., 3rd, … Zheng, J. (2016). Tailoring renal clearance and tumor targeting of ultrasmall metal nanoparticles with particle density. *Angewandte Chemie International Edition English*, *55*(52), 16039–16043.

Tepel, M., Aspelin, P., & Lameire, N. (2006). Contrast-induced nephropathy: A clinical and evidence-based approach. *Circulation*, *113*(14), 1799–1806.

Tian, G., Zhang, X., Zheng, X., Yin, W., Ruan, L., Liu, X., … Zhao, Y. (2014). Multifunctional Rbx WO3 nanorods for simultaneous combined chemo-photothermal therapy and photoacoustic/CT imaging. *Small*, *10*(20), 4160–4170.

Torchilin, V. P., Frank-Kamenetsky, M. D., & Wolf, G. L. (1999). CT visualization of blood pool in rats by using long-circulating, iodine-containing micelles. *Academic Radiology*, *6*(1), 61–65.

Toy, R., Bauer, L., Hoimes, C., Ghaghada, K. B., & Karathanasis, E. (2014). Targeted nanotechnology for cancer imaging. *Advanced Drug Delivery Reviews*, *76*, 79–97.

Wang, F., Gao, F., Lan, M., Yuan, H., Huang, Y., & Liu, J. (2009). Oxidative stress contributes to silica nanoparticle-induced cytotoxicity in human embryonic kidney cells. *Toxicology in Vitro*, *23*(5), 808–815.

Wang, J., & Liu, G. (2018). Imaging nano-bio interactions in the kidney: Toward a better understanding of nanoparticle clearance. *Angewandte Chemie International Edition English*, *57*(12), 3008–3010.

Wang, X., Wang, J., Pan, J., Zhao, F., Kan, D., Cheng, R., … Sun, S. K. (2019). Rhenium sulfide nanoparticles as a biosafe spectral CT contrast agent for gastrointestinal tract imaging and tumor theranostics in vivo. *ACS Applied Materials & Interfaces*, *11*(37), 33650–33658.

Wang, Y., Wu, Y., Liu, Y., Shen, J., Lv, L., Li, L., … Chai, Z. (2016). BSA-mediated synthesis of bismuth sulfide nanotheranostic agents for tumor multimodal imaging and thermoradiotherapy. *Advanced Functional Materials*, *26*(29), 5335–5344.

Weigel, S., Berkemeyer, S., Girnus, R., Sommer, A., Lenzen, H., & Heindel, W. (2014). Digital mammography screening with photon-counting technique: Can a high diagnostic performance be realized at low mean glandular dose? *Radiology*, *271*(2), 345–355.

Wen, L., Chen, L., Zheng, S., Zeng, J., Duan, G., Wang, Y., … Gao, M. (2016). Ultrasmall biocompatible WO3- x nanodots for multi-modality imaging and combined therapy of cancers. *Advanced Materials*, *28*(25), 5072–5079.

Willemink, M. J., & Noël, P. B. (2019). The evolution of image reconstruction for CT-from filtered back projection to artificial intelligence. *European Radiology*, *29*(5), 2185–2195.

Willemink, M. J., Persson, M., Pourmorteza, A., Pelc, N. J., & Fleischmann, D. (2018). Photon-counting CT: Technical principles and clinical prospects. *Radiology*, *289*(2), 293–312.

Wu, R., Hu, X., & Wang, J. (2018). Concise review: Optimized strategies for stem cell-based therapy in myocardial repair: Clinical translatability and potential limitation. *Stem Cells*, *36*(4), 482–500.

Xu, J., Yu, M., Carter, P., Hernandez, E., Dang, A., Kapur, P., … Zheng, J. (2017). In vivo X-ray imaging of transport of renal clearable gold nanoparticles in the kidneys. *Angewandte Chemie International Edition English*, *56*(43), 13356–13360.

Yang, S., Li, Z., Wang, Y., Fan, X., Miao, Z., Hu, Y., … Yu, M. (2018). Multifunctional Bi@PPy-PEG core-shell nanohybrids for dual-modal imaging and photothermal therapy. *ACS Applied Materials & Interfaces*, *10*(2), 1605–1615.

Ye, K., Qin, J., Peng, Z., Yang, X., Huang, L., Yuan, F., … Lu, X. (2014). Polyethylene glycol-modified dendrimer-entrapped gold nanoparticles enhance CT imaging of blood pool in atherosclerotic mice. *Nanoscale Research Letters*, *9*(1), 529.

Yhee, J. Y., Lee, S., & Kim, K. (2014). Advances in targeting strategies for nanoparticles in cancer imaging and therapy. *Nanoscale*, *6*(22), 13383–13390.

Yong, Y., Cheng, X., Bao, T., Zu, M., Yan, L., Yin, W., … Zhao, Y. (2015). Tungsten sulfide quantum dots as multifunctional nanotheranostics for in vivo dual-modal image-guided photothermal/radiotherapy synergistic therapy. *ACS Nano*, *9*(12), 12451–12463.

You, Q., Sun, Q., Yu, M., Wang, J., Wang, S., Liu, L., … Li, N. (2017). BSA-bioinspired gadolinium hybrid-functionalized hollow gold nanoshells for NIRF/PA/CT/MR quadmodal diagnostic imaging-guided photothermal/photodynamic cancer therapy. *ACS Applied Materials & Interfaces*, *9*(46), 40017–40030.

Yu, N., Wang, Z., Zhang, J., Liu, Z., Zhu, B., Yu, J., … Chen, Z. (2018). Thiol-capped Bi nanoparticles as stable and all-in-one type theranostic nanoagents for tumor imaging and thermoradiotherapy. *Biomaterials*, *161*, 279–291.

Yu, S., Droege, M., Segal, B., Kim, S. H., Sanderson, T., & Watson, A. D. (2000). Cuboidal W3S4 cluster complexes as new generation X-ray contrast agents. *Inorganic Chemistry*, *39*(6), 1325–1328.

Yu, S. B., & Watson, A. D. (1999). Metal-based X-ray contrast media. *Chemical Reviews*, *99*(9), 2353–2378.

Zhang, G., Naha, P. C., Gautam, P., Cormode, D. P., & Chan, J. M. W. (2018). Water-dispersible bismuth-organic materials with computed tomography contrast properties. *ACS Applied Bio Materials*, *1*(6), 1918–1926.

Zhang, Y., Wen, S., Zhao, L., Li, D., Liu, C., Jiang, W., … Zhao, Q. (2016). Ultrastable polyethyleneimine-stabilized gold nanoparticles modified with polyethylene glycol for blood pool, lymph node and tumor CT imaging. *Nanoscale*, *8*(10), 5567–5577.

Zhou, C., Long, M., Qin, Y., Sun, X., & Zheng, J. (2011). Luminescent gold nanoparticles with efficient renal clearance. *Angewandte Chemie International Edition English*, *50*(14), 3168–3172.

Zhou, Z., Kong, B., Yu, C., Shi, X., Wang, M., Liu, W., … Yang, S. (2014). Tungsten oxide nanorods: An efficient nanoplatform for tumor CT imaging and photothermal therapy. *Scientific Reports*, *4*, 3653.

Zhu, J., Fu, F., Xiong, Z., Shen, M., & Shi, X. (2015). Dendrimer-entrapped gold nanoparticles modified with RGD peptide and alpha-tocopheryl succinate enable targeted theranostics of cancer cells. *Colloids and Surfaces B: Biointerfaces*, *133*, 36–42.

Zimmerman, K. C., & Schmidt, T. G. (2015). Experimental comparison of empirical material decomposition methods for spectral CT. *Physics in Medicine and Biology*, *60*(8), 3175–3191.